

See discussions, stats, and author profiles for this publication at: <http://www.researchgate.net/publication/249643868>

Projected changes wave climate from a multi-model ensemble

ARTICLE *in* NATURE CLIMATE CHANGE · JANUARY 2013

Impact Factor: 15.3 · DOI: 10.1038/NCLIMATE1791

CITATIONS

47

DOWNLOADS

142

VIEWS

126

5 AUTHORS, INCLUDING:



[Mark A. Hemer](#)

The Commonwealth Scientific and Industri...

59 PUBLICATIONS 493 CITATIONS

[SEE PROFILE](#)



[Nobuhito Mori](#)

Kyoto University

225 PUBLICATIONS 1,023 CITATIONS

[SEE PROFILE](#)



[Alvaro Semedo](#)

University of Lisbon

54 PUBLICATIONS 195 CITATIONS

[SEE PROFILE](#)



[Xiaolan L. Wang](#)

Environment Canada

89 PUBLICATIONS 2,900 CITATIONS

[SEE PROFILE](#)

Projected changes in wave climate from a multi-model ensemble

Mark A. Hemer^{1*}, Yalin Fan², Nobuhito Mori³, Alvaro Semedo^{4,5} and Xiaolan L. Wang⁶

Future changes in wind-wave climate have broad implications for the operation and design of coastal, near- and off-shore industries and ecosystems, and may further exacerbate the anticipated vulnerabilities of coastal regions to projected sea-level rise^{1,2}. However, wind waves have received little attention in global assessments of projected future climate change. We present results from the first community-derived multi-model ensemble of wave-climate projections. We find an agreed projected decrease in annual mean significant wave height (H_s) over 25.8% of the global ocean area. The area of projected decrease is greater during boreal winter (January–March, mean; 38.5% of the global ocean area) than austral winter (July–September, mean; 8.4%). A projected increase in annual mean H_s is found over 7.1% of the global ocean, predominantly in the Southern Ocean, which is greater during austral winter (July–September; 8.8%). Increased Southern Ocean wave activity influences a larger proportion of the global ocean as swell propagates northwards into the other ocean basins, observed as an increase in annual mean wave period (T_M) over 30.2% of the global ocean and associated rotation of the annual mean wave direction (θ_M). The multi-model ensemble is too limited to systematically sample total uncertainty associated with wave-climate projections. However, variance of wave-climate projections associated with study methodology dominates other sources of uncertainty (for example, climate scenario and model uncertainties).

There is increasing evidence for climate-driven historical variability of wind-wave climate over at least the satellite altimeter era^{3–6} with trends in wave height seen in observing ship records over the past half-century⁷. Observed variability in wave climate is attributable to changes in global marine wind fields (for example, refs 6,8) and with projected future changes in these winds⁹, climate-driven changes in wave climate are anticipated. However, coupled atmosphere–ocean general circulation models (GCMs) generally do not yet include wind-wave-dependent parameterizations¹⁰, and wave parameters are therefore not available amongst the standard suite of climate variables used to characterize the climate system^{2,11}. As a result, the understanding of projected changes in wave climate is limited relative to other climatological parameters such as temperature, precipitation or sea level.

A growing number of studies have considered how global wave climate may respond to projected future climate scenarios with increased greenhouse-gas concentrations^{12–14} (Y. F. *et al.* and A. S. *et al.* manuscripts in preparation). These studies have been carried out independently, using different methods to investigate projected future wave-climate changes. Within each individual

study, only a limited number of climate model simulations were investigated owing to limited study scope and/or availability of suitable climate model data. Individual studies are therefore unable to fully quantify the uncertainty of projected changes in wave climate. Here, our primary aim is to use results contributed to the Coordinated Ocean Wave Climate Project¹¹ (COWCLIP) to quantitatively compare the magnitude of projected changes derived from five independent studies and to determine the level of agreement between available projections of wave climate. Four of the five contributions (ref. 13, Y. F. *et al.* (manuscript in preparation), ref. 14 and A. S. *et al.* (manuscript in preparation), hereafter MEA10, FEA12, HEA12 and SEA12, respectively) take a dynamical approach. In these studies, high-resolution atmospheric GCMs are used to dynamically downscale the results of a forcing atmosphere–ocean GCM. Surface winds from the high-resolution atmospheric model are then used to force a spectral wind-wave model. The fifth contribution¹² (WS06) uses a statistical approach to develop wave-climate projections, exploiting a relationship between mean sea-level pressure (MSLP) and H_s . Details of each contribution are given in the Supplementary Information.

Contributing studies^{12–14} (Y. F. *et al.* and A. S. *et al.*, manuscripts in preparation) have assessed the performance of each model to represent the historical wave climate on an individual basis. Here, we assess model skill of each contribution using pattern correlation and root-mean-square deviations (r.m.s.d.) between model wave fields from the representative historical time-slice with wave reanalysis data (from ERA-Interim¹⁵ and C-ERA40 (ref. 16)—see Supplementary Information). Model skill is strongly dependent on the approach of each study to develop wave-climate fields (which we term methodology), as shown by clustering of ensemble members from each study (Fig. 1). Methodology refers to whether the approach taken is dynamical (for example, HEA12, MEA10, FEA12 and SEA12) or statistical (for example, WS06), but also the specifics of the combination of downscaling atmospheric GCM and wave models used in dynamical studies, or the statistical model developed for statistical studies. The r.m.s.d. in H_s between the models and ERA-Interim and C-ERA40 is typically less than 0.6 m regardless of study, region of comparison (Global, G; Northern Hemisphere, NH; Equatorial, Eq; or Southern Hemisphere—see Methods for definition) or season (annual, January–March (JFM) or July–September (JAS) mean). The MEA10 member shows an H_s r.m.s.d. of 0.55 m, with the lowest H_s correlations in the ensemble of 0.45 (annual equatorial mean, relative to ERA-Interim; Fig. 1a) reflecting the large bias observed in this model in the equatorial region (see Supplementary Information). All other ensemble members exhibit high (>0.85) H_s

¹CSIRO Wealth from Oceans National Research Flagship and the Centre of Australian Weather and Climate Research: A Partnership between CSIRO and the Bureau of Meteorology, GPO Box 1538, Hobart, Tasmania 7001, Australia, ²Princeton University/GFDL, Princeton, New Jersey 08536, USA, ³Disaster Prevention Research Institute, Kyoto University, Kyoto 611-0011, Japan, ⁴Escola Naval, CINAV, Lisbon 2810-001, Portugal, ⁵Department of Earth Sciences, Uppsala University, Uppsala 752 36, Sweden, ⁶Climate Research Division, Science and Technology Branch, Environment Canada, Toronto, Ontario, M3H 5T4, Canada. *e-mail: mark.hemer@csiro.au.

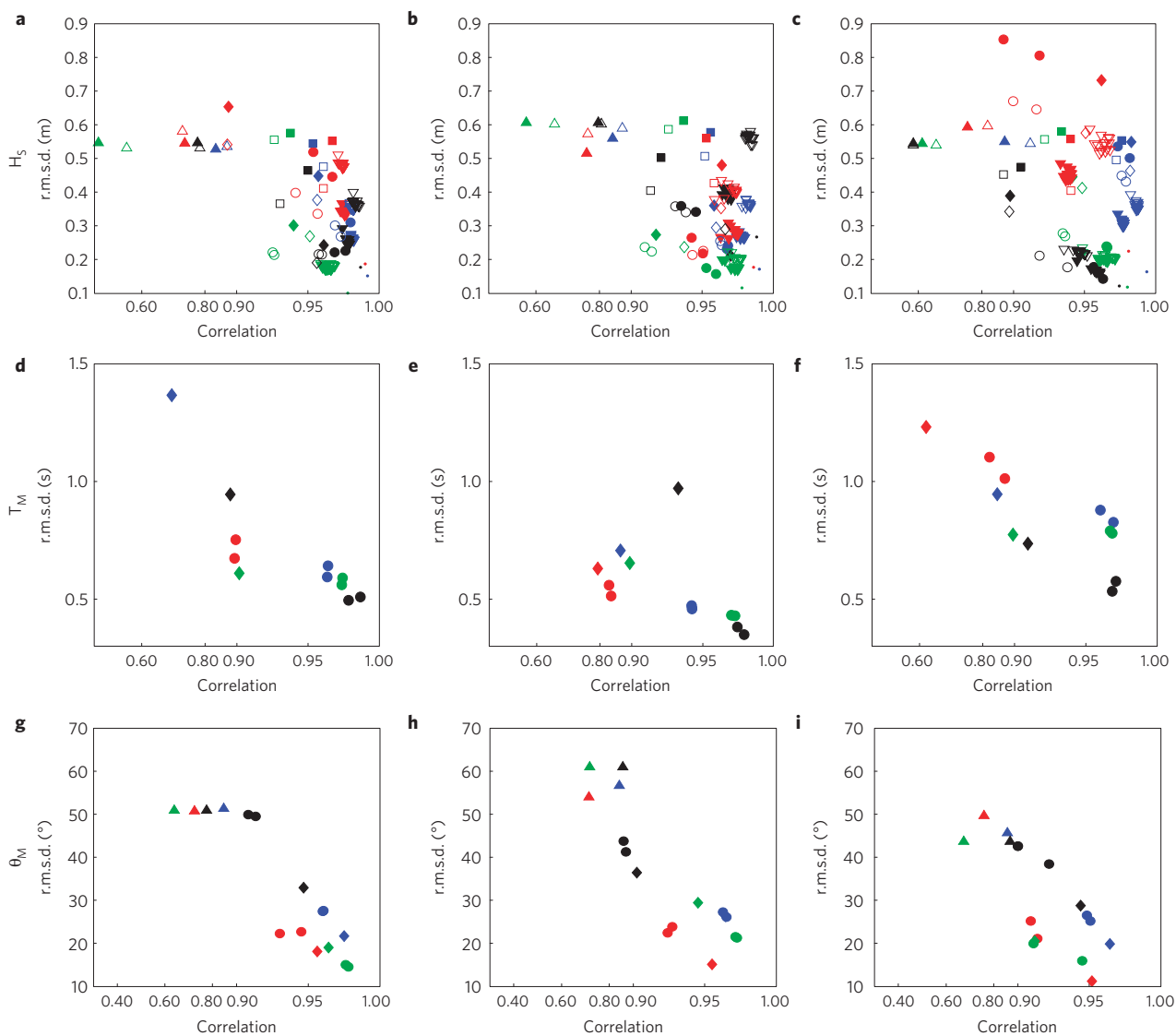


Figure 1 | Correlation and r.m.s.d. of H_S , T_M and θ_M for models with respect to ERA-Interim and C-ERA40. a–i, Left, centre and right plots show comparisons of annual, JFM and JAS, respectively. Global comparisons are indicated in blue, Southern Hemisphere in red, equatorial region in green and Northern Hemisphere in black. HEA12 runs (circles); MEA10 (uptriangles); FEA12 (diamonds); SEA12 (squares) and WS06 (downtriangles). Dots designate r.m.s.d. and correlation between ERA-Interim (filled markers) and C-ERA40 (open markers). Bias relative to ERA-Interim for each individual model is included in the Supplementary Information. Note the nonlinear scale on the abscissa of each subplot.

correlation with reanalyses (Fig. 1). WS06 ensemble members show closest agreement with reanalyses because they were produced using ERA-40 reanalysis sea-level pressure and H_S relationships, although r.m.s.d. up to 0.6 m is observed (JAS SH mean, relative to C-ERA40; Fig. 1c). A positive bias in SH H_S during JAS found in HEA12 ensemble members (see Supplementary Information) leads to the largest r.m.s.d. observed in the ensemble (0.8–0.85 m relative to ERA-Interim; Fig. 1c), but correlation remains relatively high (0.91 and 0.88). Further assessment of model skill including assessment of interannual variability bias and historical trends is given in the Supplementary Information.

Three of the five contributing groups (MEA10, FEA12 and HEA12) provided T_M and θ_M fields for inter-comparison. Strong negative biases in T_M and strong zonal biases in θ_M are observed in the MEA10 historical time-slices (see Supplementary Information). This is characteristic of strong dissipation of low-frequency (swell) waves in this model. As with H_S , the remaining members cluster by methodology, with a tendency for lower correlations/larger r.m.s.d. in the SH during the austral winter (JAS; Fig. 1f). These differences

are observed as a positive (negative) T_M bias in the SH in the HEA12 (FEA12) members (see Supplementary Information).

Correlation and r.m.s.d. values for θ_M show a similar level of agreement as for T_M . Correlation values range between 0.62 (MEA12 Eq annual and JAS means; Fig. 1g) to 0.96 (HEA12 Eq annual mean; Fig. 1g). The values for the r.m.s.d. range from 11° (FEA12 SH JAS mean; Fig. 1i) to over 60° (MEA12 NH and Eq JFM mean; Fig. 1h). Both HEA12 and FEA12 models show similar characteristics with a bias of approximately 15° towards increased zonal (easterly) flow in the equatorial regions, and an increased southerly component in the Southern Ocean (see Supplementary Information).

Signals of projected change in H_S show agreement between models over considerable portions of the global ocean (Fig. 2). Changes in the multi-model annual mean H_S (\bar{H}_S) show a consistent projected decrease among models over a larger area (25.8% of the global ocean) and consistent increases over a smaller area (7.1% of the global ocean; Table 1). Projected increases in \bar{H}_S are generally limited to the Southern Ocean, associated with a

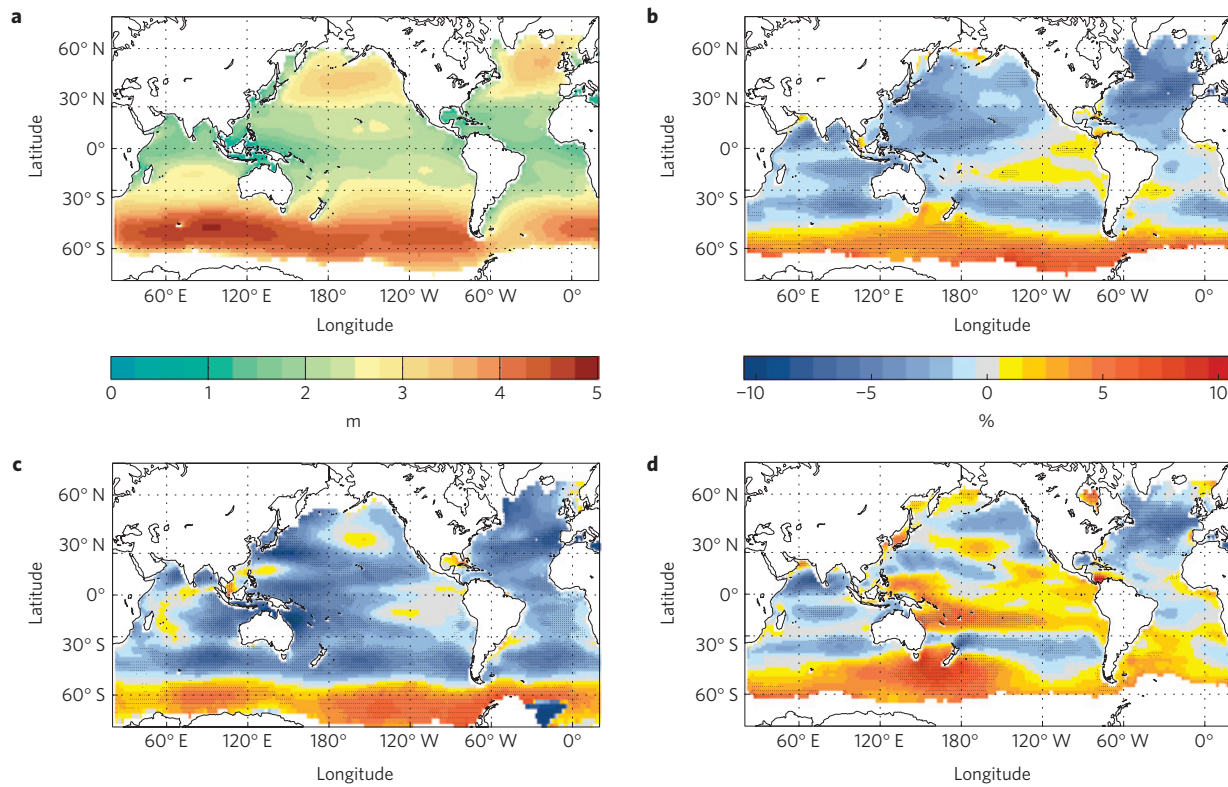


Figure 2 | Projected future changes in multi-model averaged significant wave height. **a**, Averaged multi-model annual significant wave height (H_s , m) for the time-slice representing present climate ($\sim 1979-2009$). **b-d**, Averaged multi-model projected changes in annual (**b**), JFM (**c**) and JAS (**d**) mean H_s for the future time-slice ($\sim 2070-2100$) relative to the present climate time-slice ($\sim 1979-2009$) (% change). Stippling denotes areas where the magnitude of the multi-model ensemble mean exceeds the inter-model standard deviation. Results for individual models are included in the Supplementary Information.

Table 1 | Percentage area of global ocean where projected increase/decrease is robust within the multi-model ensemble.

Annual		JFM		JAS	
Percentage area of robust projected increase	Percentage area of robust projected decrease	Percentage area of robust projected increase	Percentage area of robust projected decrease	Percentage area of robust projected increase	Percentage area of robust projected decrease
H_s	7.1	25.8	4.9	38.5	8.8
T_M	30.2	19.0	8.7	44.6	33.6
θ_M	18.4	19.7	8.95	21.4	17.1

See Methods for definition used for robustness. Increase (decrease) in direction (θ_M) corresponds to clockwise (anti-clockwise) rotation.

strengthening of the westerlies¹⁷. Small areas of projected increase in the tropical eastern Pacific Ocean are associated with an increasing Southern Ocean swell component (substantiated by increasing T_M —see below). An agreed decrease in \overline{H}_s across all models is projected in all other ocean basins, particularly in the subtropics. In the North Atlantic, this decrease spans all seasons, generally consistent with projected wind changes in the Coupled Model Intercomparison Project, Phase 3 (CMIP3; ref. 18) multi-model data set⁹. In the boreal winter (JFM; Fig. 2c), the relative area of projected decrease is enhanced (38.5% (4.9%) of oceans show projected decrease (increase); Table 1). In the austral winter however (JAS; Fig. 2d), regions of projected decrease and increase are comparable at about 8% of the global ocean (Table 1). A notable region of agreed projected increase is observed in the southern Pacific trade wind zone, consistent with projected strengthening of easterly trade winds in the winter subtropics seen in the CMIP3 multi-model data set¹⁹.

Although the area of projected H_s increase is relatively limited in extent (to the Southern Ocean), the projected increase in T_M over a much larger area (30.2 % of the global ocean shows an increase in annual mean T_M ; Table 1 and Fig. 3) shows the extended influence of enhanced Southern Ocean wave generation propagating as swell northwards across the global ocean. This Southern Ocean influence on T_M is large during the austral winter (33.6% of the global ocean shows a robust projected increase in JAS mean T_M ; Table 1), but not during the boreal winter (44.6% of the global ocean shows a robust projected decrease in JFM mean T_M ; Table 1).

Shoreline position is equally sensitive to directional changes as to changes in wave height²⁰. Projected anticlockwise rotations of θ_M (Fig. 4) are predominantly located on the northern side of the extratropical storm belts (westerly regions) in the Southern Ocean, North Pacific and Atlantic basins (19.7%, 21.4% and 12.7% of the global ocean in annual, JFM and JAS means, respectively). These correspond with an increased southerly component of θ_M

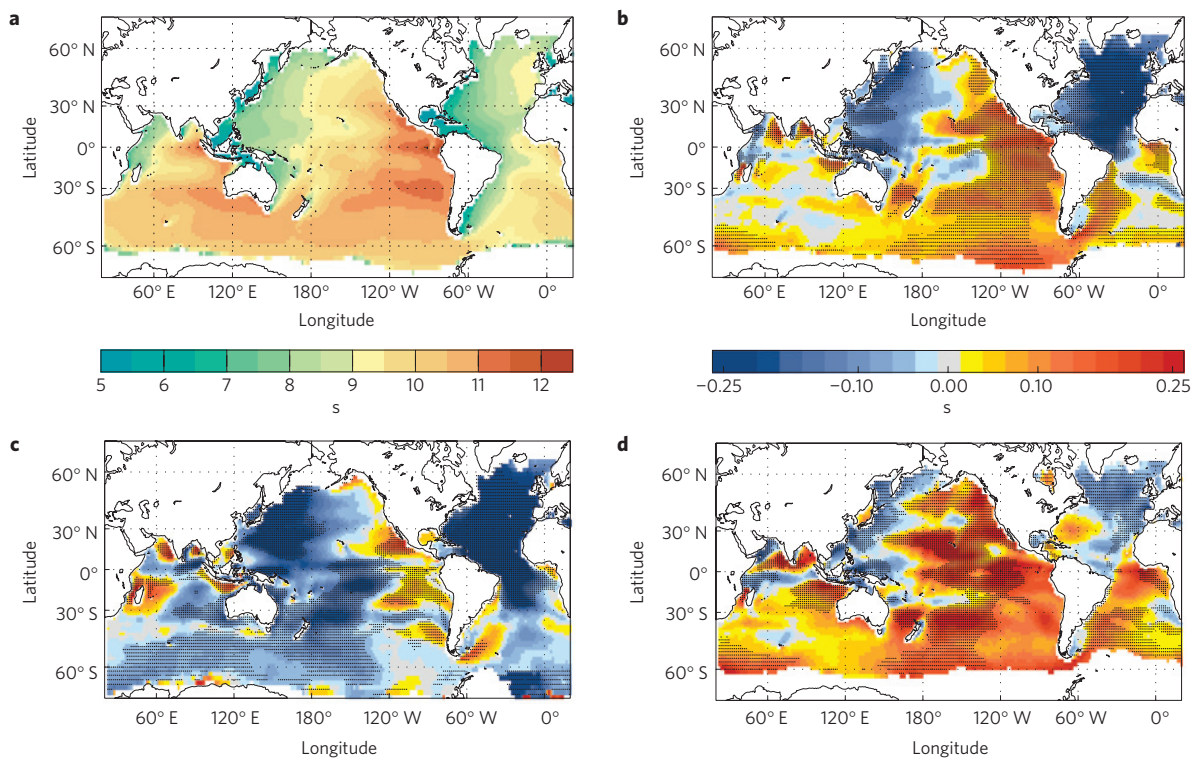


Figure 3 | Projected future changes in multi-model averaged mean wave period. **a**, Averaged multi-model annual mean wave period (T_M , s) for the time-slice representing present climate (~1979–2009). **b–d**, Averaged multi-model projected changes in annual (**b**), JFM (**c**) and JAS (**d**) mean T_M for the future time-slice (~2070–2100) relative to the present climate time-slice (~1979–2009) (absolute change, seconds). Mean wave period from only two groups is used (HEA12 and FEA12). Stippling denotes areas where the two models agree on the sign of change. Results for individual models, including MEA10, are included in the Supplementary Information.

associated with projected poleward shifts of the storm tracks¹⁷. In the southern equatorial region, the projected clockwise rotation in θ_M is associated with more southerly wind waves. In the northern equatorial region, the projected clockwise rotation is associated with more easterly wind waves. Both features are consistent with a larger contribution of Southern Ocean swell.

A seasonal signal of projected changes in θ_M is observed in the equatorial Pacific. In the boreal winter (JFM; Fig. 4b), anticlockwise rotation (up to 10°) of the waves generated by the easterly trade wind in the northern equatorial Pacific infers an increased northerly component (propagating away from the northern extratropical storm belt). In the austral winter (JAS; Fig. 4c), a projected anticlockwise rotation in the southern equatorial Pacific suggests an increased southeasterly component, consistent with projected strengthening of trade winds in the region associated with stronger projected sea-surface temperature increase on the Equator relative to the South Pacific²¹.

Features of projected change in wave climate observed in our study are consistent with a broader understanding of wave-climate variability as a response to projected changes in atmospheric circulation. See Supplementary Information for a discussion on the changes in climate regimes that are potentially responsible for the dominant features of projected wave-climate change.

A range of projected scenarios is evident within the ensemble (see Supplementary Information) owing to the many levels of uncertainties in future wave-climate projections that stem from different sources, introduced at various stages in the modelling process. Our data set is best described as an ensemble of opportunity and it is recognized that extracting policy-relevant information and quantifying uncertainties from such a data set is difficult²². Our ensemble presents many challenges, in that it is too limited to sample the full range of uncertainty. Simulations within the ensemble

span different forcing scenarios, GCMs, downscaling and wave modelling approaches, insufficiently sampled to resolve dominant sources of variance. Limited analysis (see Supplementary Information) suggests the dominant source of variance of projected wave-climate change in the available studies is a function of methodology. WS06 (ref. 12) found the uncertainty due to differences among three climate models they assessed was much larger than that due to differences among the three forcing scenarios considered. From this study, we suggest the third level of uncertainty they discussed but did not quantify (that is, the uncertainty due to different approaches taken to generate regional-scale climate-change information from global climate model simulations, such as the use of different regional climate models, or dynamical versus statistical downscaling approaches, or different statistical approaches) is greater than forcing and model uncertainties.

The present ensemble of wave-climate projections was derived from CMIP3 GCM simulations. The low temporal and spatial resolution archives from CMIP3 had limited application for wind-wave studies. CMIP5 (ref. 23) provides a data set that will enable improved systematic sampling of uncertainty in wave-climate projections. Although the wave-climate community is hopeful, it remains to be seen whether CMIP5-derived projections will enable sources of variance within the wind-wave ensemble to be better quantified.

Until recently, coastal impacts of climate-change studies have been preoccupied with the influence of sea-level rise. There is a need to determine how other driving forces in the coastal zone (for example, waves and storm surges) will respond to a changing climate to aid these studies. Here, we have shown that wave climate is projected to change over large areas of the global ocean in a future climate, but a broad range of uncertainty surrounds these projections dominated by downscaling methodologies. Storm surge

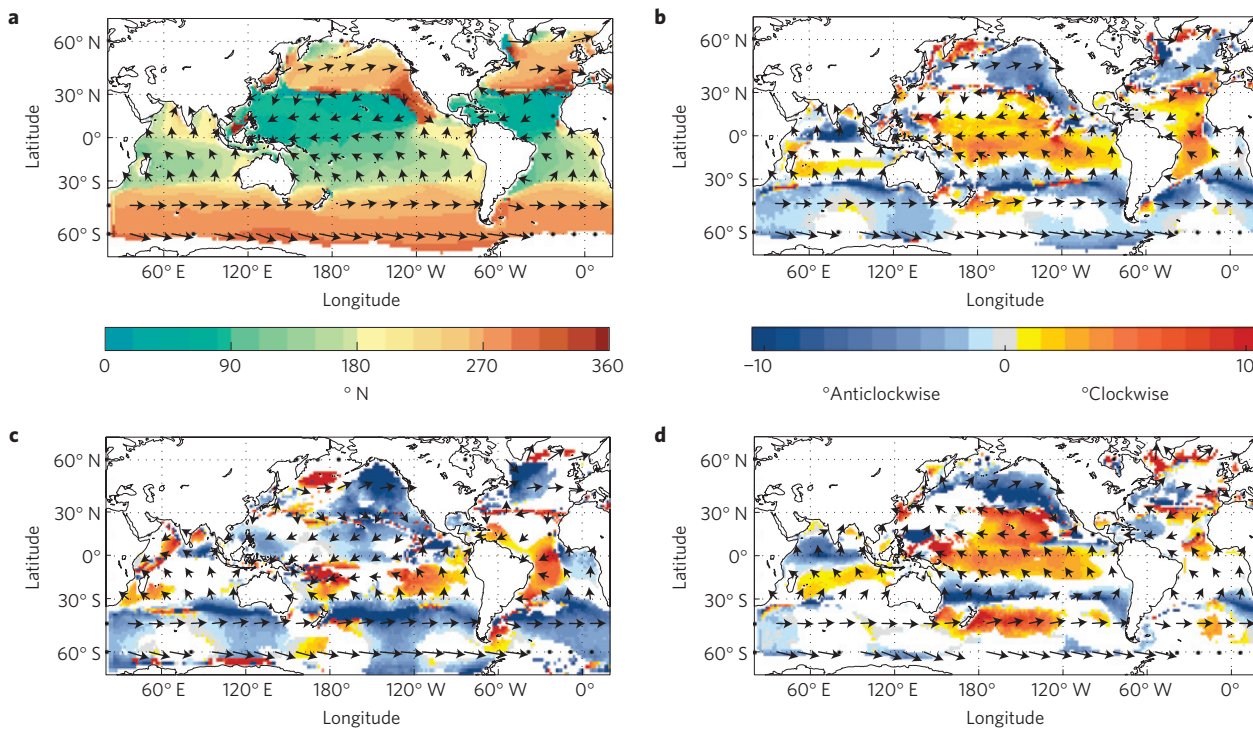


Figure 4 | Projected future changes in multi-model averaged mean wave direction. **a**, Averaged multi-model annual mean wave direction (θ_M , ° N) for a historical time-slice (~1979–2009). The vectors indicate the directions shown in the left colour bar. **b–d**, Averaged multi-model projected changes in annual (**b**), JFM (**c**) and JAS (**d**) mean wave direction (θ_M) for a projected time-slice (~2070–2100) relative to historical climate (absolute change, ° clockwise). The vector direction denotes θ_M for the historical time-slice. Colour denotes the magnitude of projected change according to the right colour bar. Mean wave directions from three groups are used (HEA12, MEA10 and FEA12). Only areas where groups agree on the sign of change are coloured. Results for individual models are included in the Supplementary Information.

climate projections probably exhibit these same characteristics. Interannual variability of waves and surges is a dominant source of shoreline position variance²⁴, in some cases exceeding the influence of projected sea-level rise²⁰. Low confidence in projected changes of wind-wave characteristics (height, length and directions) casts considerable doubt on the very-high-confidence categorization that coasts will be exposed to increasing risk in a future climate²⁵.

Methods

Monthly mean H_s , mean wave period, T_M , and mean wave direction θ_M , were obtained from each wave-climate projection data set (Supplementary Table SM2). The only parameter common to all data sets is the monthly mean H_s (20 ensemble members), and this parameter is the focus of the intercomparison. However, climate-change-driven impacts (offshore and/or in the coastal zone) will also probably result from changes in T_M and θ_M . T_M is available from 2 studies (4 ensemble members), and θ_M is available from 3 studies (5 ensemble members). The projected change in these limited ensembles for these wave parameters is also considered.

For each data set, annual and seasonal (JFM and JAS) means of a given wave parameter are determined from the archive of monthly values for each of the present and projected time-slices. We note discrepancies in the definition of present wave climate between studies (for example, the SEA12 present time-slice, 1959–1990, differs considerably from other studies, which have a common period 1979–2004). To aid intercomparison between studies, we assume that differences between studies for the present climate are attributable to model error, and not from non-stationarity of the wave climate.

Model skill for the present wave climate is assessed by comparison with wave fields obtained from ERA-Interim¹⁵ (1979–2009) and statistically corrected ERA-40 (ref. 16; C-ERA40, 1979–2002) reanalyses. A low bias in ERA-40 H_s (ref. 26) was reported in ref. 16, in which the statistically corrected H_s (C-ERA40) data set used in this study was developed. Dynamical biases in T_M and θ_M remain in the ERA-40 data, and we do not include these data in our study. Furthermore, owing to the general scarcity of wave data, an assimilative wave reanalysis will strongly depend on the background model, and will never be data-dominated and thus the error statistics of such a reanalysis are inhomogeneous, and cannot be estimated effectively. Annual and seasonal mean values of H_s , T_M and θ_M are determined for

the present climate at 1.5° spatial resolution from the 6-hourly archives. Climate model wave fields are interpolated onto the ERA-Interim/C-ERA40 grid before calculating r.m.s.d. and spatial correlation coefficients for each variable (H_s , T_M and θ_M) as simple measures of comparing model performance. Correlation and r.m.s.d. are calculated for each model over the present time-slice against ERA-Interim and C-ERA40 globally (G), over the regions north of 30° N (NH), between 30° N and 30° S (Eq) and south of 30° S (SH) for annual and seasonal—January–March (JFM) and July–September (JAS)—means (Fig. 1).

Changes in H_s statistics between the two (present and future) time-slices are calculated as percentage changes. Projected T_M changes are calculated as absolute values, and changes in θ_M are calculated as clockwise or anticlockwise rotation in degrees relative to the present climate mean. A multi-model mean projected change is determined. Fourteen statistical projected scenarios are available from WS06, whereas other groups contributing dynamical projections consist of just one or two projected scenarios. Hence, a uniformly weighted mean across all projected scenarios would be inappropriately weighted to the statistical projections²². The provision of wave-climate projections is in a preliminary phase, and metrics for model performance are not well established. Consequently, our objective was to limit weighting or ranking of any existing study over any other. The full ensemble was therefore reduced to 5 members, with each member consisting of the average from a given study (for example, the 14-member WS06 ensemble was reduced to a single member). This choice was made on the basis that model skill depended strongly on method (or group from which the wave field originated). Figure 1 shows clustering of results dependent on their origin. Furthermore, analysis of projected change from all individual ensemble members shows strong similarity dependent on their origin (see Supplementary Information).

For mean H_s (available from all groups), the map of mean projected change is obtained as the 5-member multi-model mean difference between projected and present climate wave fields. Stippling is shown where the multi-model mean response exceeds the model spread (measured as one standard deviation across the 5 members) as a simple measure of model agreement (Fig. 2). Distribution of means is unavailable from all studies, prohibiting a more sophisticated approach²⁷. For other parameters that were unavailable from all groups, the multi-model mean response was determined from fewer members (2 or 3 depending on variable). In these cases, stippling as a measure of model agreement is shown where all models agree on the sign of change (Figs 3 and 4). For annual and seasonal means of each wave variable, the percentage area of the global ocean that exhibits agreed (by the above definitions) projected increase and decrease was determined (Table 1).

Received 23 May 2012; accepted 22 November 2012;
published online 13 January 2013

References

- Lowe, J. A. *et al.* in *Understanding Sea-Level Rise and Variability* (eds Church, J. A. *et al.*) 326–375 (Wiley-Blackwell, 2011).
- Hemer, M. A., Wang, X. L., Church, J. R. & Swail, V. R. Coordinating global ocean wave climate projections. *Bull. Am. Meteorol. Soc.* **91**, 451–454 (2010).
- Woolf, D. K., Challenor, P. G. & Cotton, P. D. Variability and predictability of the North Atlantic wave climate. *J. Geophys. Res.* **107**, 3145 (2002).
- Hemer, M. A., Church, J. A. & Hunter, J. R. Variability and trends in the directional wave climate of the Southern Hemisphere. *Int. J. Climatol.* **30**, 475–491 (2010).
- Semedo, A., Suselj, K., Rutgersson, A. & Sterl, A. A global view on the wind sea and swell climate and variability from ERA-40. *J. Clim.* **24**, 1461–1479 (2011).
- Young, I. R., Zieger, S. & Babanin, A. V. Global trends in wind speed and wave height. *Science* **332**, 451 (2011).
- Gulev, S. K. & Grigorieva, V. Last century changes in ocean wind wave height from global visual wave data. *Geophys. Res. Lett.* **31**, L24302 (2005).
- Tokinaga, H. & Xie, S.-P. Wave- and anemometer-based sea surface wind (WASWind) for climate change analysis. *J. Clim.* **24**, 267–285 (2011).
- McInnes, K. L., Erwin, T. A. & Bathols, J. M. Global climate model projected changes in 10 m wind speed and direction due to anthropogenic climate change. *Atmos. Sci. Lett.* **12**, 325–333 (2011).
- Cavaleri, L., Fox-Kemper, B. & Hemer, M. Wind-waves in the coupled climate system. *Bull. Am. Meteorol. Soc.* **93**, 1651–1661 (2012).
- Hemer, M. A., Wang, X. L., Weisse, R. & Swail, V. R. Community advancing wind-waves climate science: The COWCLIP project. *Bull. Am. Meteorol. Soc.* **93**, 791–796 (2012).
- Wang, X. L. & Swail, V. R. Climate change signal and uncertainty in projections of ocean wave heights. *Clim. Dynam.* **26**, 109–126 (2006).
- Mori, N., Yasuda, T., Mase, H., Tom, T. & Oku, Y. Projection of extreme wave climate change under the global warming. *Hydrol. Res. Lett.* **4**, 15–19 (2010).
- Hemer, M. A., Katzfey, J. & Trenham, C. Global dynamical projections of surface ocean wave climate for a future high greenhouse gas emission scenario. *Ocean Modelling* <http://dx.doi.org/10.1016/j.ocemod.2012.09.008> (2012).
- Dee, D. P. *et al.* The ERA-Interim reanalysis: Configuration and performance of the data assimilation system. *Q. J. R. Meteorol. Soc.* **137**, 553–597 (2011).
- Sterl, A. & Caires, S. Climatology, variability and extrema of ocean waves—The web-based KNMI/ERA-40 wave atlas. *Int. J. Climatol.* **25**, 963–997 (2005).
- Arblaster, J. M., Meehl, G. A. & Karoly, D. J. Future climate change in the Southern Hemisphere: Competing effects of ozone and greenhouse gases. *Geophys. Res. Lett.* **38**, L02701 (2011).
- Meehl, G. A. *et al.* The WCRP CMIP3 multi-model dataset: A new era in climate change research. *Bull. Am. Meteorol. Soc.* **88**, 1383–1394 (2007).
- Sobel, A. H. & Camargo, S. J. Projected future changes in tropical summer climate. *J. Clim.* **24**, 473–487 (2011).
- Coelho, C., Silva, R., Veloso-Gomes, F. & Taveira-Pinto, F. Potential effects of climate change on northwest Portuguese coastal zones. *ICES J. Mar. Sci.* **66**, 1497–1507 (2009).
- Timmermann, A., McGregor, S. & Jin, F.-F. Wind effects on past and future regional sea level trends in the southern Indo-Pacific. *J. Clim.* **23**, 4429–4437 (2010).
- Knutti, R., Furrer, R., Tebaldi, C., Cermak, J. & Meehl, G. Challenges in combining projections from multiple climate models. *J. Clim.* **23**, 2739–2758 (2010).
- Taylor, K., Stouffer, R. & Meehl, G. A. An overview of CMIP5 and the experiment design. *Bull. Am. Meteorol. Soc.* **93**, 485–498 (2012).
- Kuriyama, Y., Banno, M. & Suzuki, T. Linkages among interannual variations of shoreline, wave and climate at Hasaki, Japan. *Geophys. Res. Lett.* **39**, L06604 (2012).
- Nicholls, R. J. *et al.* in *IPCC Climate Change 2007: Impacts, Adaptation and Vulnerability* (eds Parry, M. L., Canziani, O. F., Palutikof, J. P., van der Linden, P. J. & Hanson, C. E.) 315–356 (Cambridge Univ. Press, 2007).
- Uppala, S. *et al.* The ERA-40 re-analysis. *Q. J. R. Meteorol. Soc.* **131**, 2961–3012 (2005).
- Tebaldi, C., Arblaster, J. M. & Knutti, R. Mapping model agreement on future climate projections. *Geophys. Res. Lett.* **38**, L23701 (2011).

Acknowledgements

The study was conceived as part of the COWCLIP (ref. 4) project, an international collaborative working group endorsed by the World Climate Research Program and the Joint Commission on Oceanography and Marine Meteorology of the World Meteorological Organization and the UNESCO Intergovernmental Oceanographic Commission. We acknowledge the European Centre for Medium Range Weather Forecasting for the reanalysis data, and the climate modelling groups, the Program for Climate Model Diagnosis and Intercomparison (PCMDI) and the WCRP's Working Group on Coupled Modelling (WGCM) for their roles in making available the WCRP CMIP3 multi-model data set. Support of the CMIP3 data set is provided by the Office of Science, US Department of Energy. M.A.H. acknowledges the support of the Australian Climate Change Science Programme and the CSIRO Wealth from Oceans National Research Flagship. We thank all contributors to the COWCLIP project, along with J. Church for comments on an earlier version of the manuscript.

Author contributions

All authors jointly conceived the study and contributed experimental data equally. M.A.H. analysed data and prepared the manuscript, with all authors discussing results and implications and commenting on the manuscript at all stages.

Additional information

Supplementary information is available in the online version of the paper. Reprints and permissions information is available online at www.nature.com/reprints. Correspondence and requests for materials should be addressed to M.A.H.

Competing financial interests

The authors declare no competing financial interests.

Projected changes in wave climate from a multi-model ensemble

Mark A. Hemer^{1*}, Yalin Fan², Nobuhito Mori³, Alvaro Semedo^{4,5}, Xiaolan Wang⁵

¹. CSIRO Wealth from Oceans National Research Flagship and the Centre of Australian Weather and Climate Research: A Partnership between CSIRO and the Bureau of Meteorology, GPO Box 1538, Hobart, TAS 7001, Australia

². Princeton University / GFDL, Princeton, NJ, 08536, USA

³. Disaster Prevention Research Institute, Kyoto University, Kyoto, 611-0011, Japan

⁴. Escola Naval-CINAV, Lisbon, 2810-001, Portugal

⁵. Department of Earth Sciences, Uppsala University, Uppsala, 752 36, Sweden

⁶. Climate Research Division, Science and Technology Branch, Environment Canada, Toronto, ON, M3H 5T4, Canada

*Corresponding author address:

Dr Mark Hemer
Centre for Australian Weather and Climate Research:
A Partnership between CSIRO and the Bureau of Meteorology
GPO Box 1538
Hobart, TAS 7001
Australia
Email: mark.hemer@csiro.au
Tel: +61-3-6232-5017

Section 1 of the supplementary material details the datasets and models used in our study. Section 2 details our analyses of performance and projected change of each of the ensemble members available for the study. Eleven supplementary figures are included, and three supplementary tables.

1. Detailed description of data and models

1.1 Data for evaluation

1.1.1 ERA-Interim

ERA-Interim¹⁵ is the most recent global atmospheric reanalysis produced by the European Centre for Medium Range Weather Forecasts. For this study data spanning the 31-year period, 1979-2009 inclusive, is used. ERA-Interim provides gridded data products, including 3-hourly surface wave parameters (significant wave height, H_s , mean wave period, T_M , and mean wave direction, θ_M) archived on a 1.5° latitude-longitude grid. ERA-interim wave parameters are derived from a fully coupled atmosphere-wave model (wave model, WAM^{SM1}) which describes the evolution of two-dimensional wave spectra at the sea-surface, with assimilated satellite radar altimeter derived wave height data (from 1991 onwards) to adjust the model predicted wave spectra based on assumptions about the contributions of wind-sea and swell. The wave model is applied with a horizontal resolution of 110 km, with wave spectra discretized using 24 directions and 30 frequencies. The model includes several enhancements over the version used in ERA-40, including a reformulation of the dissipation source term and introduction of a scheme to parameterize unresolved bathymetry. Notable improvement of ERA-Interim wave parameters (H_s , T_M , and T_p) relative to ERA-40 were reported by Dee et al.¹⁵, with the overall quality of ERA-Interim wave fields being equivalent to the operational analysis of 2005.

1.1.2 Corrected ERA-40

Prior to ERA-Interim, the ECMWF carried out a 45-yr reanalysis of global meteorological variables spanning the period 1957-2002. This reanalysis was the first in which an ocean wind-wave model was coupled to the atmosphere, and provides one of the longest and most complete wave datasets available²⁶. To create ERA-40, a version of the ECMWF integrated forecast system that was operational in June 2001 was used, with resolution decreased to T_159m and a cheaper 3DVAR assimilation scheme. The wave model used is WAM^{SM1}. From the full spectrum, integrated parameters significant wave height, mean wave period and mean wave direction are determined, and archived at 6-hourly resolution at a spatial resolution of $1.5^\circ \times 1.5^\circ$. The wave climate from the ERA-40 dataset is well understood, following the KNMI wave atlas project^{SM2}. Sterl and Caires¹⁶ found the ERA-40 wave reanalysis tended to underestimate large wave heights, particularly in the Southern Ocean, and consequently produced a statistically corrected dataset which is used in this study, and termed the corrected ERA-40 (C-ERA40) wave height data. A complete understanding of the C-ERA40 wave climatology has been gained from prior studies^{4,5,16}, and consequently we use C-ERA40 wave heights as a benchmark in our study in addition to the updated ERA-interim dataset. We do not use ERA-40 T_M or θ_M data.

1.2 Contributing Wave Climate Models

Twenty scenarios of wave climate change are assessed in this study, derived from 5 studies. These studies are summarized below. Table SM1 summarises the five contributing studies, with further details contained in Table SM2.

1.2.1 HEA12: Hemer et al., (2012)¹⁴

Hemer et al.¹⁴ (hereafter HEA12) presented global wave climate projections derived using a dynamical approach. Two CMIP3 AOGCMs (CSIRO Mk3.5 and ECHAM5, under the SRES A2 greenhouse gas emission scenario) were dynamically downscaled to 0.5° resolution using CSIRO's cubic conformal atmospheric model, with the only forcing parameter taken from the AOGCM being bias-adjusted sea-surface temperatures. Three-hourly surface (10-m) winds (and monthly mean sea-ice concentrations) were used to force a 1° near-global implementation of the WaveWatch III spectral wave model^{SM3} for 2 time-slices: 1979-2009 representing current climate, and 2070-2099 representing a future climate scenario. Hemer et al.¹⁴ also assessed the influence of bias-adjusting forcing wind conditions. Only climatologies derived from un-adjusted forcing are considered in this study.

1.2.2 MEA10: Mori et al. (2010)¹³

Mori et al.¹³ (hereafter MEA10) presented global dynamical wind-wave projections for the SRES A1B scenario. A near-global 1.25° resolution implementation of the SWAN spectral wave model^{SM4} was forced using hourly surface (10-m) winds obtained from the 20km resolution GCM developed by MRI-JMA^{SM5}. External forcing of the GCM is obtained from an ensemble mean SST obtained from the CMIP3 GCM ensemble. Three time-slices were simulated: 1979-2004, representing present climate; 2015-2031 representing near-future climate; and 2075-2100 representing the future climate. This study considers only the present and future climate time-slices.

1.2.3 SEA12: Semedo, A., Bengtsson, L., Günther, H., Weisse, R., Beherens, A. & Sterl, A. Impact of a warmer climate on the global wave field. *Manuscript submitted for publication.*

Bengtsson et al.^{SM6-7} carried out a high-resolution (T213, 63km) version of the ECHAM5 GCM for two 32-yr time-slices at the end of the 20th (1959-1990) and 21st Centuries (2069-2100), and integrated

for the SRES A1B emission scenario. SST and sea-ice fraction forcing were provided by the ECHAM5OM coupled model runs carried out for the CMIP3. Following results showing the high resolution GCM is able to resolve surface winds with greater skill than the ERA-40 reanalysis^{SM7}, Semedo et al. (hereafter SEA12) produced dynamical global wave projections using surface (10-m) winds from the GCM to force a 0.5° resolution near-global implementation of the WAM spectral wave model for the two 32-yr time-slices.

1.2.4 FEA12: Fan, Y., Held, I. M., Lin, S. & Wang, X. Global ocean wave climate change scenarios for the end of the 21st century. *Manuscript submitted for publication*

Fan et al.^{SM8} coupled the WaveWatch III wave model to GFDL's High resolution Atmospheric Model (HiRAM). The coupled model was used to dynamically project global wave climate change in the late 21st Century under the SRES A1B scenario, with external forcing derived from SST anomalies from CMIP3 GCMs (Fan, Y., Held, I. M., Lin, S. & Wang, X. Global ocean wave climate change scenarios for the end of the 21st century. *Manuscript submitted for publication* – hereafter FEA12). Two forcing datasets were considered (two climatologies for present and projected time-slices): One using SST's derived from the GFDLcm2.1 model (*GFDL-Coupled_GFDL2.1*), and the other using SST's from an 18-member CMIP3 GCM ensemble mean SST (*GFDL-Coupled_18ens*). The global implementation of HiRAM has a horizontal resolution of approximately 50km, and the wave model is run at a resolution of 0.5°. A wave climatology for a present (1979-2009) and end of 21st Century (2070-2099) time-slice were derived from each forcing dataset.

1.2.5 WS06: Wang and Swail (2006)¹²

Wang and Swail¹² (hereafter WS06) provided statistically based projections of wave climate for three future emission scenarios (IS92a and SRES A2 and B2). Using the (un-corrected) ERA-40 reanalysis,

WS06 identified a statistical relationship between mean sea-level pressure (MSLP) and significant wave height (H_s). The statistically derived projections are less computationally intensive to compute, and are therefore able to sample a larger range of the distribution. They obtained sub-daily MSLP from 3 GCMs (HadCM3, ECHAM4, and 3 perturbed-physics ensembles from CGCM2) for the period 1958-2100 for each scenario, and exploited the derived statistical relationship to provide projections of H_s through the 21st Century. Two time-slices were used for this study: 1979-2009 representing present climate, and 2070-2099 representing the projected future climate.

2. Analysis of Projections

2.1 Evaluation of ensemble members

2.1.1 Mean Bias

Annual, JFM and JAS mean of H_s , T_M and θ_M from the present time-slice from each ensemble member were determined, where available, from each model ensemble. For H_s , maps of mean percentage bias between the annual mean H_s and ERA-Interim for each ensemble member (20) are presented in Figures SM1A-T. For ensemble members derived from studies HEA12, SEA12 and WS06, distribution of means were available to carry out a standard t-test for difference in means, to determine whether distributions of the mean wave climate were significantly different. The area of global ocean which show significantly different annual, JFM and JAS mean values (at 95% significance level) to ERA-Interim mean H_s is given in Table SM3.

For T_M , maps of mean absolute bias between the annual mean T_M and ERA-Interim for each ensemble member (5) are presented in Figures SM2A-E. For θ_M , maps of mean absolute bias between annual mean θ_M and ERA-Interim for each (5) ensemble member are presented in Figures SM3A-E.

H_s biases are variable across the ensemble (Figure SM1). Ensembles derived from dynamical studies (HEA12, MEA10, FEA12 and SEA12; Figures SM1-F) show a general positive bias, with biases of approximately 40-50% noted in the equatorial Pacific in SEA12 (Figure SM1F). MEA10 shows strong negative biases in the equatorial regions. We attribute this to insufficient swell propagating from the southern and northern storm track generation zones, which is consistent with characteristics of the SWAN wave model exhibiting high numerical dissipation of swell energy over large spatial distances^{SM9}. Ensembles derived from WS06 (the statistical study) show relative consistency with a negative bias of up to approximately 15% (on the west coast of Australia) across all members. In addition to ensemble members G-T being consistent, ensemble members A and B, and D and E, derived from the same studies, show high consistency in the spatial distribution and magnitude of bias within a study. This result suggests model performance is a property of the methodology used to develop wave projections, as opposed to climate model forcing (e.g., emission scenario, or forcing CMIP3 GCM). Table SM3 shows WS06 derived annual, JFM and JAS mean H_s fields differs significantly to corresponding means from ERA-Interim over approximately 66%, 53% and 53% of the global ocean respectively. Dynamical study derived members A, B and F for which distribution of means is available show larger areas of the global ocean with significantly different means to ERA-Interim (Table 1 of manuscript) – up to 97.6% in annual mean H_s for member F.

Biases in T_M (Figure SM2) for ensemble members A-E reflect similar characteristics as derived from the H_s biases. A strong negative bias is observed for MEA10, indicating wave periods are short in the MEA10 dataset. This is consistent with high dissipation of the swell wave component in this model. Members A and B show positive biases in wave period over large areas of the Southern hemisphere associated with the positive bias in wave heights. Members D and E show notable negative biases in the North and South Western Atlantic.

Biases in θ_M (Figure SM3) for ensemble members A-E reflect the same characteristics. The strong biases in member C (MEA10) indicate model wave directions are closely associated with dominant wind direction in the region, with little to no swell influence. Members A, B, D and E display similar characteristics, with consistent positive (clockwise) bias in wave directions in northern equatorial regions and negative (anticlockwise) bias in southern equatorial regions (overestimated easterlies in both cases). Small negative (anticlockwise) biases in wave directions are observed in storm track regions indicating overestimate of the southerly component.

2.1.2 Variability Bias

With the focus of the study being assessment of wave climate change, the skill of wave climate models to reproduce variability and change must also be assessed. An assessment of the models to represent seasonal variability is contained in the main article, by comparison of RMS and correlation between Jan-March and July-Sep mean derived values. Here, we focus on the skill of the models to represent interannual variability, and use the variability bias (derived from the time-series of annual mean H_s values – being the ratio of climate model simulated variance to the variance derived from the ERA-interim reanalysis). Figure SM4 maps the interannual variability bias for each ensemble member. We find that the magnitude of interannual variance in the dynamically derived ensemble members (HEA12, MEA10, FEA12 and SEA12), while strongly variable, is of the same order of magnitude as the variance observed in the reanalysis record. The global mean variance from the ERA-interim reanalysis is 0.014 m^2 . The global mean variance from the dynamical members varies between 0.0103 m^2 (FEA12) to 0.0174 m^2 (HEA12), with a mean value of 0.137 m^2 . The statistically derived ensemble members (WS06) however exhibit an interannual variance an order of magnitude smaller than observed in the reanalysis. The global mean variance from the statistical members (WS06) is 0.004 m^2 .

2.1.3 Historical tendencies

We assess the skill of each model to represent historical tendencies, or trends. The longest period over which data were available from the ERA-Interim reanalysis, the satellite altimeter database analysed by Young et al.⁶, and the most wave climate model ensemble members was 1992–2003. This period also has the benefit of not including the GEOSAT era of the altimeter record (1985–1989) for which poorer agreement with the reanalysis was observed. Ensembles from studies HEA12, MEA10 and WS06 are available over this period. Ensembles members from studies FEA12 and SEA12 are not included in this time-period. We calculate trends in annual mean H_s over this period, by regression against time, in each ensemble member, the weighted ensemble mean, and from the altimeter and reanalysis records. The 95% confidence interval of historical trends in these datasets is determined using a boot-strap method, repeating the regression calculation 500 times with repeat random sampling with replacement of annual mean values^{SM10}. Mapped regression slopes (trends) from the altimeter (Figure SM5a) and reanalysis (Figure SM5b) are compared against trends measured from the ensemble mean (Figure SM5d), and each individual ensemble member (Figure SM6). The time-series is short, and as a result recorded trends are not significant, except for very small areas, in any dataset (not shown). If the modeled trend does not fall within the 95% confidence interval of trends measured from the altimeter or reanalysis data, then this region is blanked (appears as white in the figure) indicating disagreement between model and ‘observed’ trend over this period. We find climate model forced wave fields possess skill in reproducing historical trends (within 95% confidence limits) of 93% of the global ocean area.

Data are available from all studies except WS06 for the time-period 1981–2000. We repeat our analysis for this period, by comparison against trends from ERA-interim reanalysis only (Figure SM5c). Altimeter data does not span this period. Over this period, we find the ensemble mean trend (Figure SM5e) shows agreement with ERA-interim (within 95% confidence levels) over 83% of the global ocean area. Trends for each ensemble member over the 1981–1990 period are shown in Figure SM7.

2.2 Projected change in wave climate for each ensemble member.

Projected changes in annual, JFM and JAS mean wave parameters for each ensemble member is determined as the difference between the associated future time-slice mean and the associated present time-slice mean. Maps of projected future percentage change in mean annual H_s for each member are presented in Figure SM4A-T. For ensemble members derived from studies HEA12, SEA12 and WS06, the significance of projected changes is assessed using a standard t-test for difference in means. The percentage area of global ocean over which the projected increase/decrease in Annual, JFM and JAS mean H_s is significant (at 95% level) is shown in Table SM3.

Maps of projected future absolute change in mean annual T_M for 5 available members are presented in Figure SM5A-E, and maps of projected future absolute change in mean annual θ_M for 5 available members are presented in Figure SM6A-E.

A large range of projected scenarios of H_s is shown amongst the ensemble members (Figure SM4A-T). While differences occur between ensemble members from the same study, there is consistency which is particularly noticeable by areas of significant projected increase/decrease shown in Table SM3 for members A and B, and G-T. Robust features of projected change, identified in the manuscript, are seen for each ensemble member. The projected Southern Ocean increase and North Atlantic decrease are particularly noticeable in the dynamical study derived members (Figure SM4A-F). The magnitude of projected change seen for each member (Figure SM4) is approximately a factor 5 less than the bias for corresponding member (Figure SM1), indicating a low signal to noise ratio.

Projected changes in T_M vary widely across the available 5-member ensemble, suggesting low confidence in the projected future changes of this variable. For example, HEA12 derived members

indicated a projected future increase in T_M in the Indian Ocean. FEA12 derived members project an increase in T_M in this region. Figure SM2 shows this to be a region where HEA12 overestimates T_M and FEA underestimates T_M (by similar magnitudes). The projected change signal is an order of magnitude smaller than the bias in this region.

We see in all ensemble members that the projected change signal of H_s and T_M do not display the same spatial distribution. Such agreement might occur if the global wave field were dominated by single-peaked spectra, e.g. simple cases of fetch-limited wave-growth or fully developed wind-seas. Under these conditions, non-dimensionalised H_s and T_M (using wind speed and gravity) vary independently under conditions of active growth, following the usual JONSWAP relations of Hasselmann et al. SM11. However, in the more normal open ocean conditions consisting of multiple sea-states (i.e., sea and swell), this dependent relationship no longer holds. Consequently, projected changes in H_s and T_M do not display the same spatial distributions. Our results are in agreement with prior studies^{SM12,SM13} which have shown that waves are rarely in wind-wave equilibrium, with swell dominating the global wave field.

Projected changes in θ_M show a relatively consistent signal between ensemble members. Projected changes seem to be large and noisy in regions that separate strong directional change, such as the subtropical ridges. This characteristic was similarly observed in projected changes in surface winds⁹. These results suggest the limited extent of robust change reported in the manuscript is attributable to relatively small spatial shifts in features of change. This is problematic when the objective is to determine regional climate information (e.g., analysis of a single grid cell to represent a point locality).

This study has assessed projected changes in the mean integrated wave field only. It is acknowledged that different components of the wave spectrum will respond differently to projected

changes in climate depending on location. In some locations, the wind-driven sea component of the wave field may be exposed to change, while the swell component remains unchanged. Conversely, local wind-sea may remain stationary, but swell influences are projected to change. Studies underway are beginning to resolve these differences which are critical to understanding the wind-wave driven impacts of climate change. Furthermore, this study has assessed only the mean wave climate, and it is the extreme wave climate which is of high interest to many coastal hazard studies. Preliminary analyses suggest that the extreme wave climate responds similarly to the mean wave climate, but biases and associated uncertainties are greater again. Increased effort in understanding how climate change will influence extreme wave events is required if valuable, policy relevant information is to be derived from wave climate projection studies.

2.3 Mechanisms for change.

A projected increase in Southern Ocean H_s is the strongest signal of change observed in the study ensemble. The dominant mode of historical variability of the Southern Hemisphere wave climate is significantly correlated with the Southern Annular Mode (SAM)⁴. Projected increase of Southern Ocean wave generation, and a larger contribution of Southern Ocean swell propagating northwards, is consistent with a projected trend in SAM towards its positive polarity, as seen for future high emission scenarios¹⁷. Positive polarity of SAM is associated with a poleward shift of the Southern Hemisphere storm tracks and increase in the westerly jet¹⁷, which translates to increased generation of wind-waves in the region, which can propagate northwards away from the generation region into the global ocean as swell. During the 21st Century, increases in greenhouse gas concentration will continue to shift the SAM towards positive values, while ozone recovery will have the opposite effect of pushing SAM towards negative values¹⁷. Our ensemble considers only high greenhouse gas emission scenarios (a combination of SRES A1B and A2), with the consequent response consistent with a shift to more positive SAM.

Another dominant feature of projected change in our ensemble is a projected decrease in wave heights in the North Atlantic Ocean. In the North Atlantic, a large fraction of wave height variability is related to the North Atlantic Oscillation (NAO)³. More than half the CMIP3 models exhibit a projected positive trend in the North Atlantic Oscillation^{SM14}, and the projected decrease in wave heights in the central North Atlantic are true to this relationship. However, a projected increase in the ensemble mean wave heights in the Northern Seas is not observed, which might be expected with a projected strengthening of NAO. Referring to individual ensembles (Figure SM8), we see a projected increase is common to several ensemble members, but the mean change signal is dominated by the strong projected decrease from HEA12.

We observe an increase in wave heights in the equatorial South Pacific Ocean during the southern Trades season (JAS). Timmerman et al.²¹ found reduced warming in the south-eastern tropical Pacific was accompanied by an intensification of the south-easterly trades in a 14-member ensemble of CMIP3 GCMs for an SRES A1B scenario, consistent with the projected increase in wave heights in this region. A strong, well-established, relationship exists between El-Niño –Southern Oscillation (ENSO) and the Pacific wave climate^{4,SM15}, with larger wave heights experienced in the central equatorial Pacific during positive phases of El-Niño. While much uncertainty surrounds future projections of El-Nino variability, the projected changes in wave height are consistent with a weak shift towards conditions which may be described as El-Niño-like^{SM14}.

2.4 Sources of uncertainty

It is recognized that the ensemble of opportunity used in this study introduces several limitations. Several sources of uncertainty are associated with the ensemble, namely forcing, GCM, downscaling methodology and wave model approaches, but the ensemble is too small to systematically sample

these multiple sources, with very little required overlap of forcing scenarios or GCMs. In some cases, temporal overlap within time-slices is limited. The root-mean-square difference between projected future annual mean H_S and present time-slice annual mean H_S was determined for each ensemble member. Numerous potential diagnostics were assessed to determine whether wave climate change could be resolved by broader climate change characteristics. No relationship with scenario, GCM, magnitude of change per year, or magnitude of 21st Century projected surface temperature change (e.g., Figure SM7), was identified. The only common feature for magnitude of projected change (measured by RMSD) was the origin of the ensemble member, with members generally clustering together according to the methodology used to derive the projections (i.e., by study). Interestingly members C and D have similar response when derived from ensemble mean SST's for the A1B scenario, but this serves to further demonstrate the limitation of our ensemble in adequately quantifying sources of variance. The study therefore concludes that the dominant source of uncertainty within the current available ensemble of global wave climate projections is derived from the downscaling methods (e.g., RCM, dynamical vs statistical methods) used to develop the wave climate projections.

Supplementary Acknowledgements

We thank Alex Babanin of Swinburne University for altimeter database.

Supplementary References

- ^{SM1}. Komen, G.J., Cavaleri, L., Donelan, M., Hasselmann, K., Hasselmann, S., Janssen, P.A.E.M., (Eds.), Dynamics and Modelling of Ocean Waves, Cambridge (1994)
- ^{SM2}. Sterl, A. and Caires, S., Climatology, Variability and Extrema of Ocean Waves - The Web-based KNMI/ERA-40 Wave Atlas. *Int. J. Climatology*, **25(7)**, 963-997, doi:10.1029/joc.1175, (2005)
- ^{SM3}. Tolman H., User manual and system documentation of WAVEWATCH-III, version 3.14. NOAA/NWS/NCEP/MMAB Technical Note 276, 194 pp. (2009)
- ^{SM4}. Booij, N., Ris, R.C. and Holthuijsen, L.H., A third generation wave model for coastal regions, Part I: Model description and validation, *J. Geophys. Res.*, **104(C4)**, 7649-7666, (1999)
- ^{SM5}. Kitoh, A., Ose, T., Kurihara, K., Kusunoki, S., Sugi, M. and KAKUSHIN Team-3 Modeling Group, Projection of changes in future weather extremes using super-high-resolution global and regional atmospheric models in the KAKUSHIN Program: Results of preliminary experiments, *Hydrol. Res. Lett.*, **3**, 49–53, doi:10.3178/hrl.3.49, (2009)
- ^{SM6}. Bengtsson, L., Hodges, K.I., Esch, M., Keenlyside, N., Kornbleuh, L., Luo, J.-J., and Yamagata, T., How many tropical cyclones change in a warmer climate?, *Tellus*, **59A**, 539-561, (2007)
- ^{SM7}. Bengtsson, L., Hodges, K.I., and Keenlyside, N., Will extratropical storms intensify in a warmer climate?, *J. Climate*, **22**, 2276-2301 doi: 10.1175/2008JCLI2678.1, (2009)
- ^{SM8}. Fan, Y., Lin, S-J., Held, I. M., Yu, Z. & Tolman, H. L. Global ocean surface wave simulation using a coupled atmosphere-wave model. *J. Clim.* **25**, 6233-6252 (2012).
- ^{SM9}. Rogers, W.E., Hwang, P.A. and Wang, D.W., Investigation of wave growth and decay in the SWAN model: Three regional-scale applications. *Journal of Physical Oceanography*, **33(2)**, 366-389 (2003)
- ^{SM10}. Efron, B., The jackknife, the bootstrap, and other resampling plans. 38. Society of Industrial and Applied Mathematics CBMS-NSF Monographs. ISBN 0-89871-179-7. 1982.

^{SM11}. Hasselmann K., T.P. Barnett, E. Bouws, H. Carlson, D.E. Cartwright, K. Enke, J.A. Ewing, H. Gienapp, D.E. Hasselmann, P. Kruseman, A. Meerburg, P. Müller, D.J. Olbers, K. Richter, W. Sell, and H. Walden. Measurements of wind-wave growth and swell decay during the Joint North Sea Wave Project (JONSWAP), Ergänzungsheft zur Deutschen Hydrographischen Zeitschrift Reihe, A(8) (Nr. 12), p.95, 1973.

^{SM12}. Hanley, K. E., S. E. Belcher, and P. P. Sullivan. A global climatology of wind-wave interaction, *J. Phys. Oceanogr.*, 40(6), 1263-1282, doi:10.1175/2010JPO4377.1. 2010

^{SM13}. Semedo, A., K. Sušelj, A. Rutgersson, A. Sterl. A Global view on the wind sea and swell climate and variability from ERA-40. *J. Climate*, 24, 5, 1461-1479. 2010.

^{SM14}. Meehl, G.A., T.F. Stocker, W.D. Collins, P. Friedlingstein, A.T. Gaye, J.M. Gregory, A. Kitoh, R. Knutti, J.M. Murphy, A. Noda, S.C.B. Raper, I.G. Watterson, A.J. Weaver and Z.-C. Zhao. Global Climate Projections. In: *Climate Change 2007: The Physical Science Basis. Contribution of Working Group I to the Fourth Assessment Report of the Intergovernmental Panel on Climate Change* [Solomon, S., D. Qin, M. Manning, Z. Chen, M. Marquis, K.B. Averyt, M. Tignor and H.L. Miller (eds.)]. Cambridge University Press, Cambridge, United Kingdom and New York, NY, USA. 2007

^{SM15}. Izquierdo, C., F. J. Méndez, M. Menéndez, and I. J. Losada. Global extreme wave height variability based on satellite data, *Geophys. Res. Lett.*, 38, L10607, doi:10.1029/2011GL047302. 2011.

List of supplementary Tables

Table SM1. Summary of the contributions to phase 1 of the Coordinated Ocean Wave Climate Projections study.

Model	Hemer et al. 2012 ¹⁶	Mori et al. 2010 ¹⁴	Fan et al. 2012 ¹⁵	Semedo et al. 2012 ¹⁷	Wang and Swail, 2006 ¹³
Abbrev.	HEA12	MEA10	FEA12	SEA12	WS06
Scenario	SRES A2	SRES A1b	SRES A1b	SRES A1b	SRES A2, B2, and IS92a
GCM(s)	ECHAM5 CSIRO Mk3.5	CMIP3 23m ens. mean	1. CMIP3 18m ens. Mean 2. GFDL-CM2.1	ECHAM5 (high-res ^{SM7})	1. HadCM3 2. ECHAM4 3. CGCM2 (3 PPE)
Forcing	CCAM	MRI-AGCM-3.1S (20km GCM)	Coupled GFDL-	-	-
Model	WaveWatch III	SWAN		WAM	Empirical Statistical Downscaling
Historical	1979-2009	1979-2005	1979-2009	1959-1990	1979-2009
time-slice					
Projected	2070-2099	2075-2099	2070-2099	2059-2100	2070-2099
time-slice					
No. Ens.	2	1	2	1	14

Table SM2. Wave climate ensemble members available for the study. Further details in Table 1 of manuscript.

Ident	Study	Scenario	GCM	Vars	ΔT (°C) [#]
A	HEA12	A2	ECHAM5	H_s, T_M, D_M	4
B	HEA12	A2	Mk3.5	H_s, T_M, D_M	3.1
C	MEA10	A1B	23 EM ¹	H_s, T_M^*, D_M	2.65
D	FEA12	A1B	18 EM ¹	H_s, T_M, D_M	2.65
E	FEA12	A1B	GFDLcm2.1	H_s, T_M, D_M	2.53
F	SEA12	A1B	ECHAM5(hr)	H_s	3.69
G	WS06	A2	CGCM (II1)	H_s	4.3
H	WS06	A2	CGCM (II2)	H_s	4.3
I	WS06	A2	CGCM (II3)	H_s	4.3
J	WS06	B2	CGCM (II1)	H_s	2.75
K	WS06	B2	CGCM (II2)	H_s	2.75
L	WS06	B2	CGCM (II3)	H_s	2.75
M	WS06	IS92a	CGCM (II1)	H_s	4.3
N	WS06	IS92a	CGCM (II2)	H_s	4.3
O	WS06	IS92a	CGCM (II3)	H_s	4.3
P	WS06	A2	ECHAM4	H_s	3.5
Q	WS06	B2	ECHAM4	H_s	2.5
R	WS06	A2	HadCM3	H_s	3.9
S	WS06	B2	HadCM3	H_s	2.5
T	WS06	IS92a	HadCM3	H_s	3.9

¹ EM is CMIP-3 ensemble mean. 18 is from 18 members, 23 from 23 members.

* T_M from MEA10 shows large biases, and is dismissed from analysis.

DT values derived from Figure 10.5 of IPCC AR4 WG1 report for CMIP-3 models. Values for models prior to CMIP3 derived from Figure 9.6 of IPCC TAR.

Table SM3. Percentage area of global ocean where model mean H_s is significantly different (at 95% CI) to ERA-interim mean H_s (% Area s.d. ERA). Percentage area of global ocean where projected future mean H_s is significantly different (at 95% CI) to the historical mean H_s (% Area sig. increase, and % Area of significant decrease).

Ident	Annual			JFM			JAS		
	% Area s.d ERA	% Area sig inc	% Area sig dec	% Area s.d ERA	% Area sig inc	% Area sig dec	% Area s.d ERA	% Area sig inc	% Area sig dec
A	83.6	19	51.0	70.1	1.0	57.5	76.1	24.8	27.8
B	83.0	4.1	85.5	73.9	5.3	81.9	75.4	2.3	63.1
C	-	-	-	-	-	-	-	-	-
D	-	-	-	-	-	-	-	-	-
E	-	-	-	-	-	-	-	-	-
F	97.6	23.7	30.5	93.1	8.7	47.1	90.9	46.5	8.3
G	66.1	34.5	30.3	53.2	28.9	24.0	54.6	28.4	26.9
H	66.1	33.5	28.1	53.6	30.5	24.0	53.1	25.7	23.8
I	66.2	34.3	25.8	50.7	29.3	22.8	57.1	27.2	24.6
J	66.1	21.2	20.8	53.1	16.8	18.5	54.3	16.9	17.7
K	66.2	18.6	19.1	54.5	16.4	15.9	53.7	16.9	15.6
L	66.1	20.9	23.6	50.2	18.0	18.6	56.0	15.3	15.6
M	66.3	30.4	27.7	53.7	30.9	20.7	54.3	18.6	23.0
N	66.1	31.2	27.6	54.6	33.1	20.4	53.6	20.3	24.7
O	66.2	33.9	26.8	52.3	32.5	22.5	55.2	19.3	25.3
P	66.0	41.4	18.6	55.3	22.6	30.2	54.1	42.7	10.0
Q	66.1	42.3	17.8	56.0	22.0	26.6	55.5	36.0	9.6
R	65.6	35.0	16.9	54.6	20.9	28.2	55.3	39.1	11.7
S	66.0	26.3	14.7	53.0	20.1	23.7	57.2	24.8	10.1
T	65.3	39.8	15.2	52.0	26.5	20.4	53.3	32.6	14.0

List of Supplementary Figures

Figure SM1. Annual mean percentage bias is annual mean H_S (%). Bias is determined as $H_{S,\text{climate}} - H_{S,\text{ERA-Interim}}$. Each subplot is for a given ensemble member detailed in Table SM1.

Figure SM2. Annual mean absolute bias is annual mean T_M (s). Bias is determined as $T_{M,\text{climate}} - T_{M,\text{ERA-Interim}}$. Each subplot is for a given ensemble member detailed in Table SM1.

Figure SM3. Annual mean absolute bias is annual mean θ_M ($^{\circ}$ clockwise). Bias is determined as $\theta_{M,\text{climate}} - \theta_{M,\text{ERA-Interim}}$. Each subplot is for a given ensemble member detailed in Table SM1.

Figure SM4. Interannual variability bias of annual mean H_S . Ratio of variance of annual mean H_S from ensemble member relative to variance of annual mean H_S from ERA-Interim. Log10 scale. Each subplot is for a given ensemble member detailed in Table SM1.

Figure SM5. Historical tendencies (regression coefficient of annual mean H_S against time; m/yr) for a) Altimeter measured H_S over period 1992-2003; b) ERA-interim reanalysis H_S over period 1992-2003; c) ERA-interim reanalysis H_S over period 1981-1990; d) limited model ensemble mean H_S over period 1992-2003, includes HEA12, MEA10 and WS06 members; e) limited model ensemble mean H_S over period 1981-1990, includes HEA12, MEA10, FEA12 and SEA12 members. For subplots d) and e), regions marked in white denote areas where regression coefficient does not fall in 95% confidence interval from ‘observational’ (altimeter or reanalysis) data.

Figure SM6. Historical tendencies (regression coefficient of annual mean H_S against time; m/yr) from models over period 1992-2003. Each subplot is for a given ensemble member detailed in Table SM1. Regions marked in white denote areas where regression coefficient does not fall in 95% confidence interval from ‘observational’ (altimeter or reanalysis) data.

Figure SM7. Historical tendencies (regression coefficient of annual mean H_S against time; m/yr) from models over period 1981-2000. Each subplot is for a given ensemble member detailed in Table SM1. Regions marked in white denote areas where regression coefficient does not fall in 95% confidence interval from ‘observational’ (altimeter or reanalysis) data.

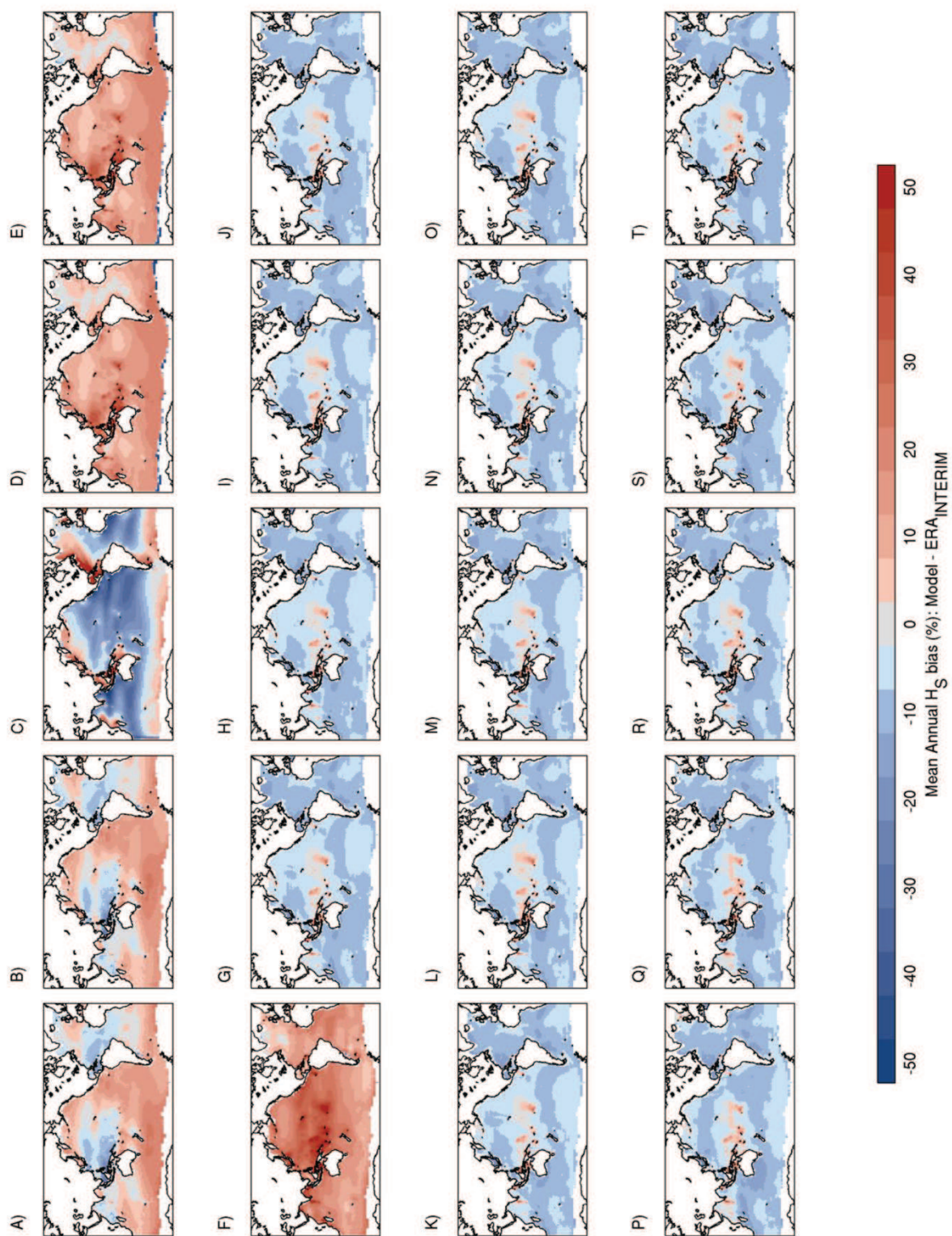
Figure SM8. Projected future percentage change in annual mean H_S (%). Bias is determined as $H_{S,\text{future}} - H_{S,\text{present}}$. Only regions where change is significant at 95% confidence level are colored. Each subplot is for a given ensemble member detailed in Table SM1.

Figure SM9. Projected future change in annual mean T_M (s). Bias is determined as $T_{M,\text{future}} - T_{M,\text{present}}$. Only regions where change is significant at 95% confidence level are colored, except C), for which no significance level could be determined. Each subplot is for a given ensemble member detailed in Table SM1.

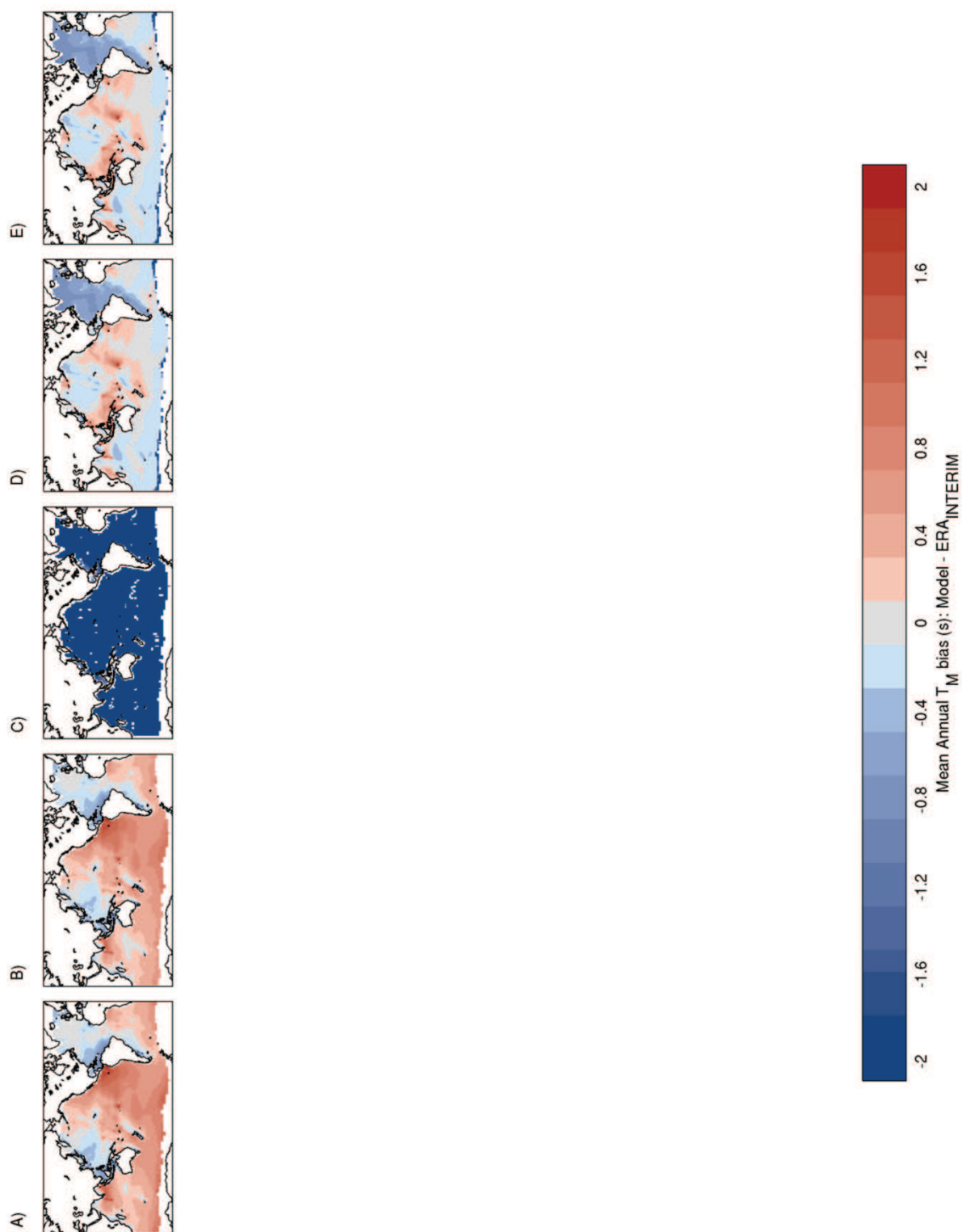
Figure SM10. Projected future percentage change in annual mean θ_M ($^{\circ}$ clockwise). Change is determined as $\theta_{M,\text{future}} - \theta_{M,\text{present}}$. Only regions where change is significant at 95% confidence level

are colored, except C), for which no significance level could be determined. Each subplot is for a given ensemble member detailed in Table SM1.

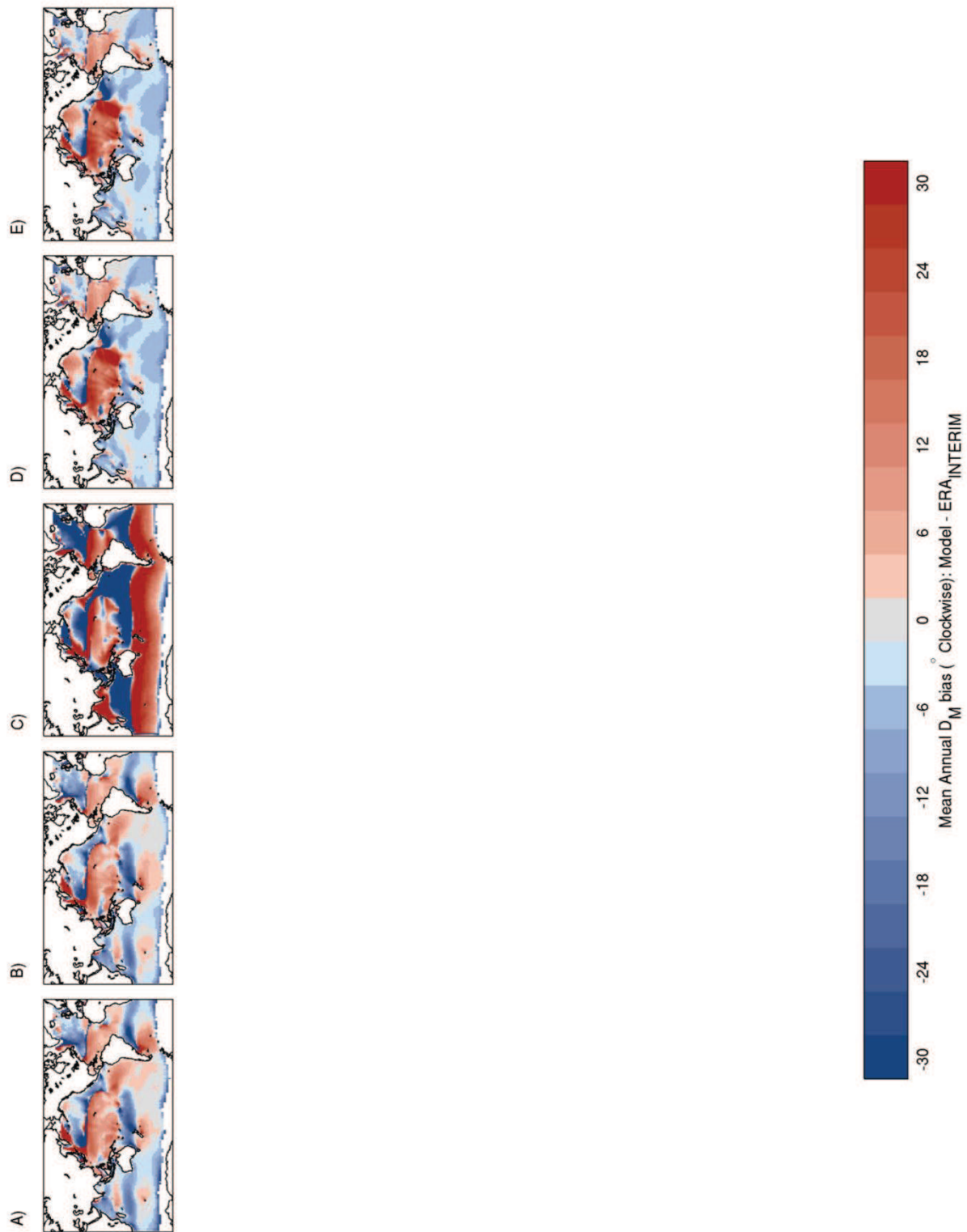
Figure SM11. RMSD between present and future time-slice mean (a) annual, (b) JFM and (c) JAS HS (m) vs 21st Century change in global mean surface temperature of the associated parent GCM of each ensemble member.



FigureSM1



FigureSM2



FigureSM3

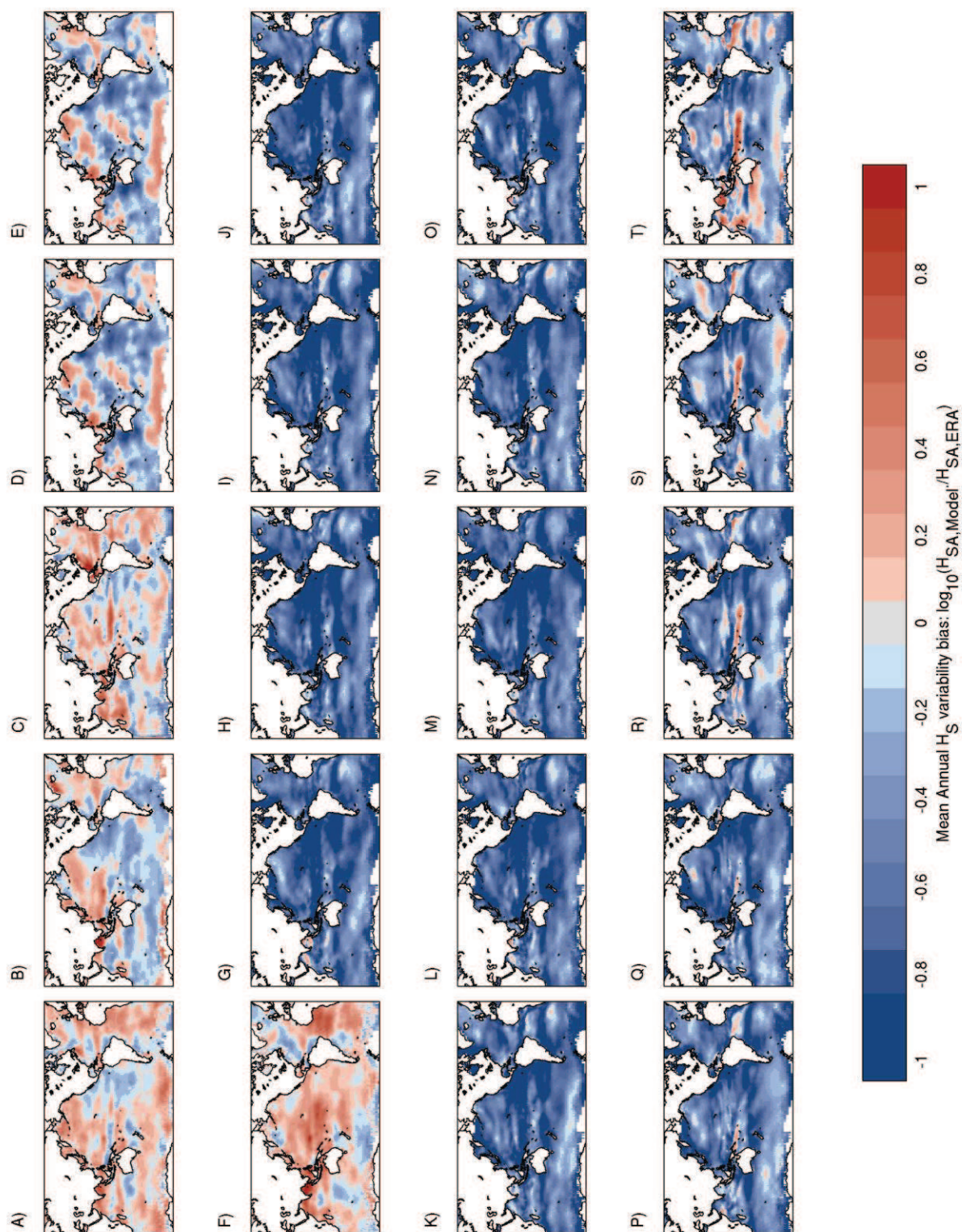


Figure SM4

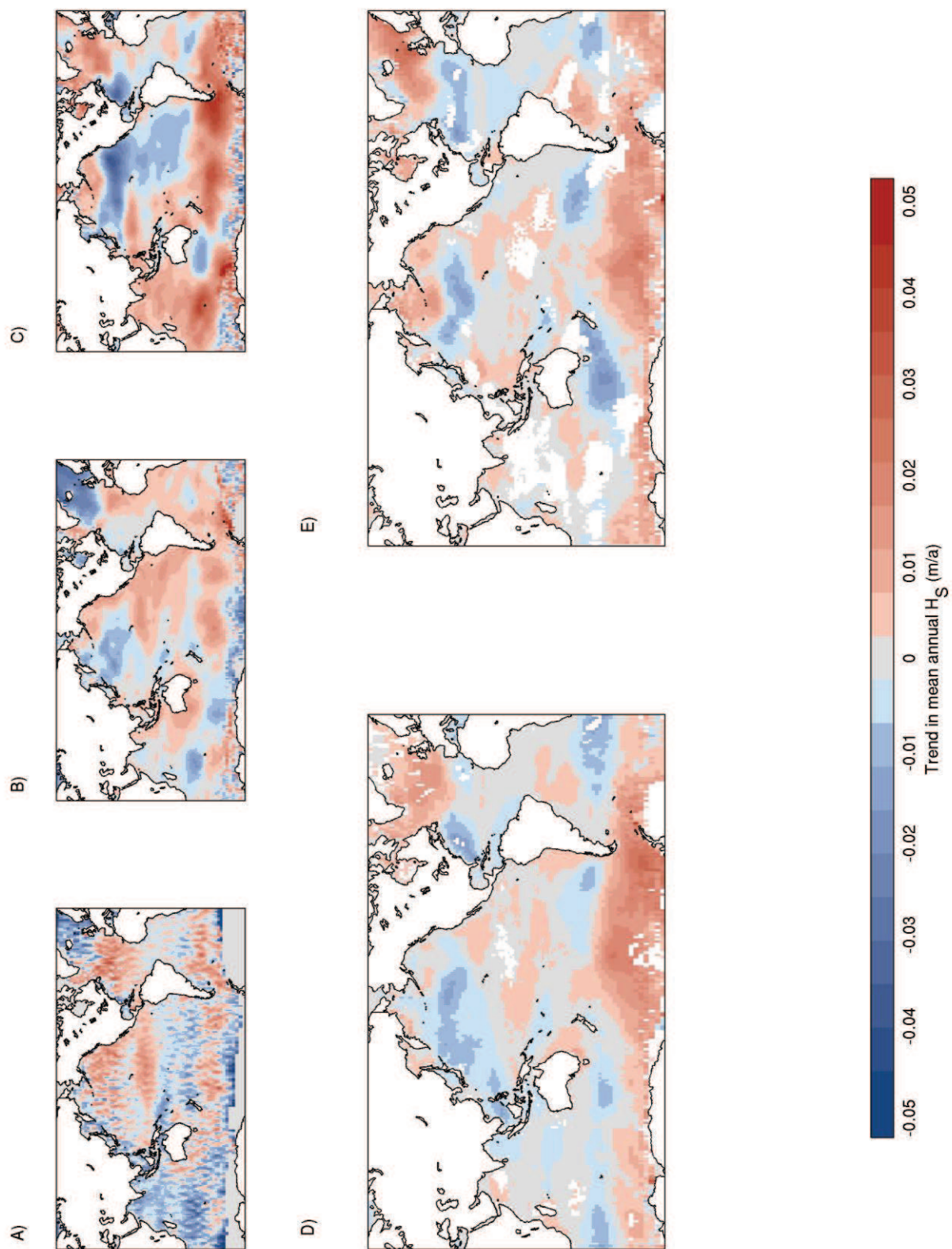


Figure SM5

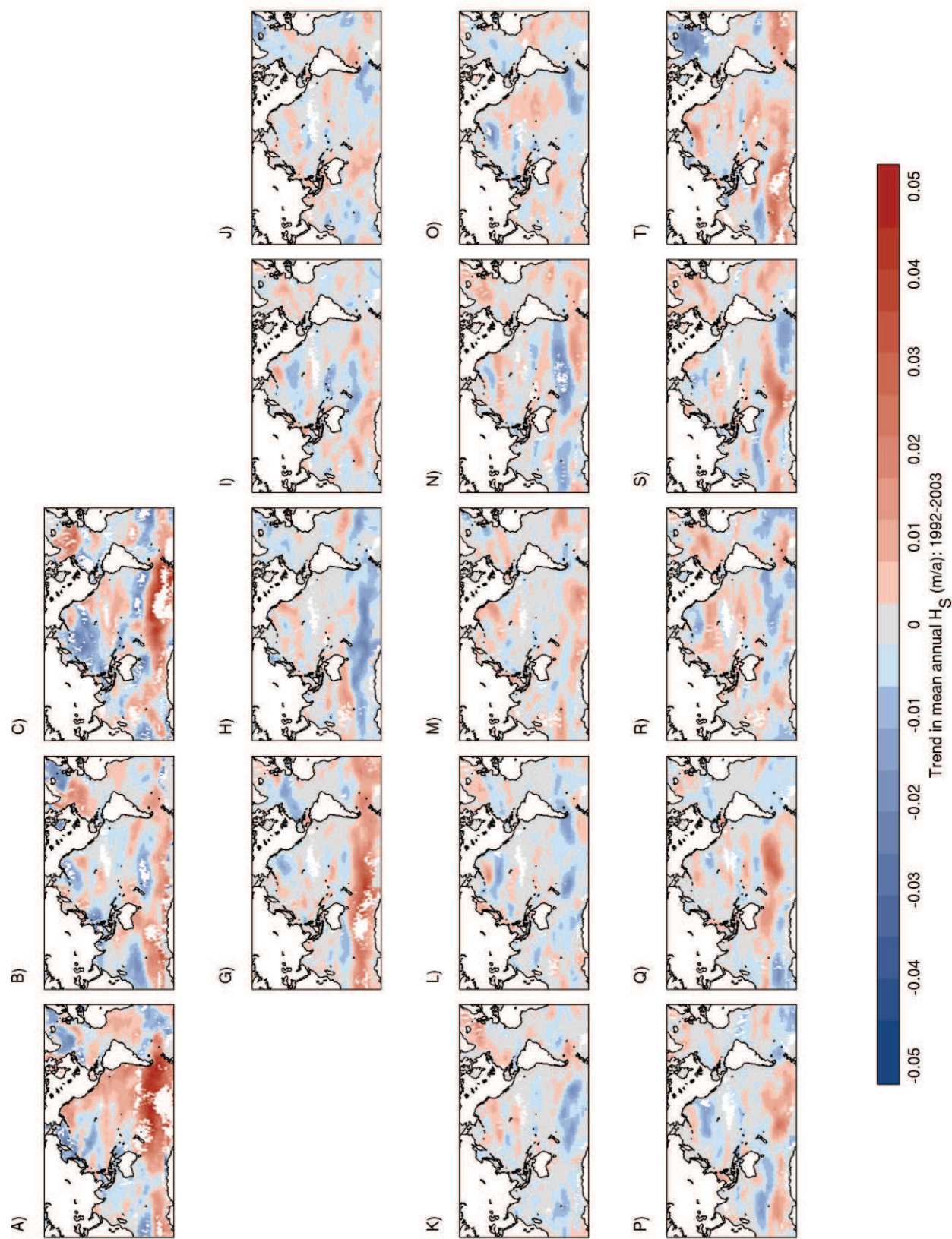


Figure SM6

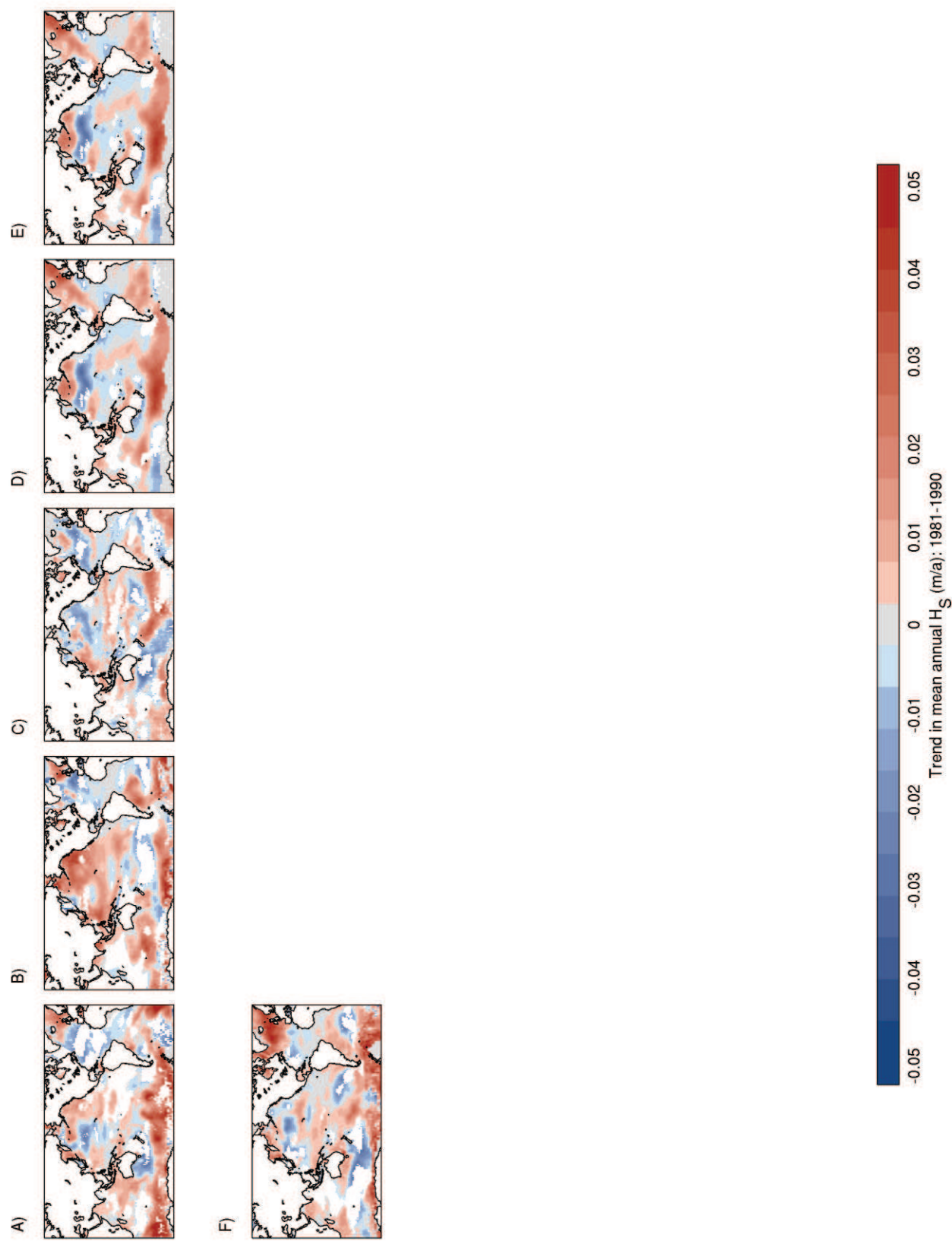


Figure SM7

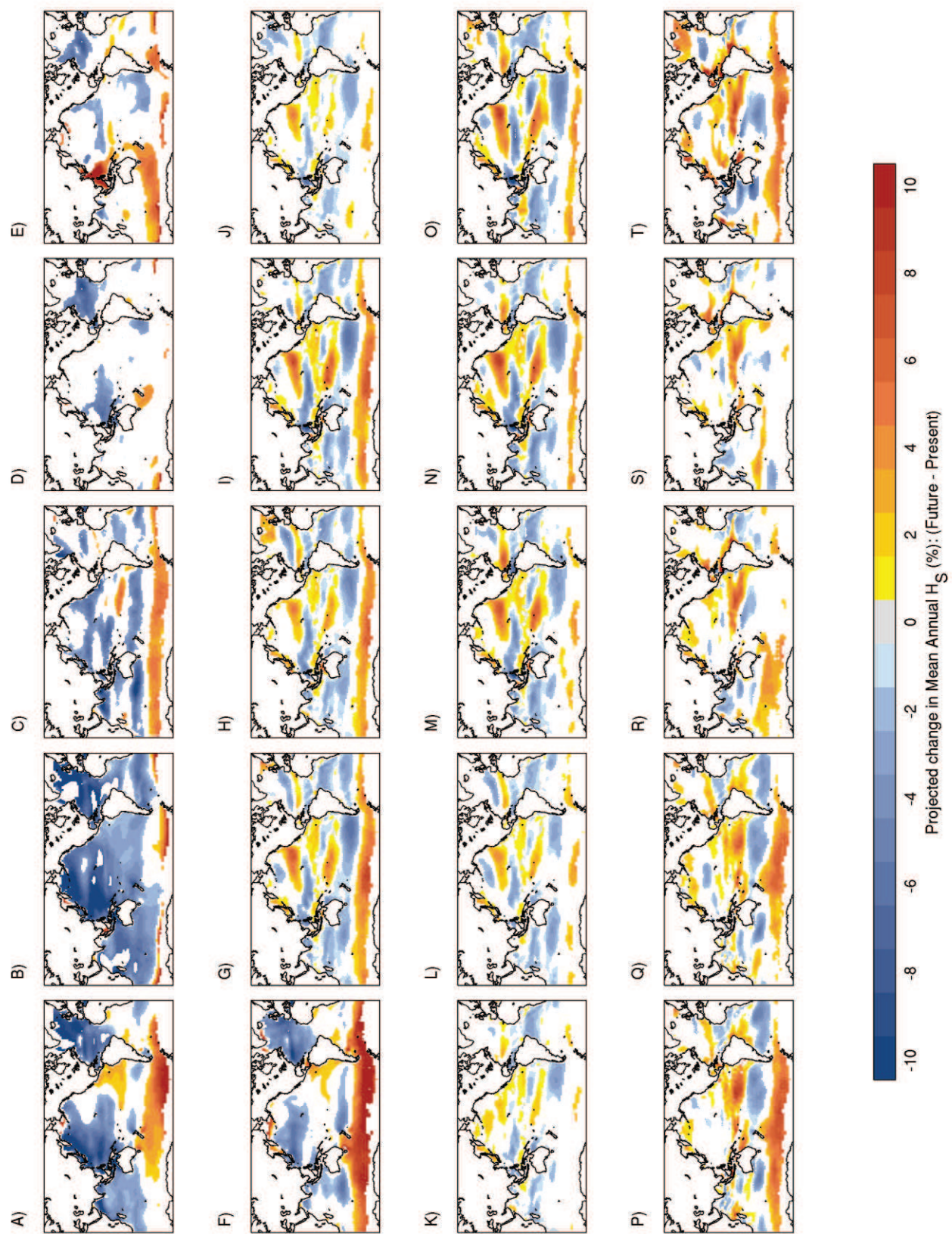


Figure SM8

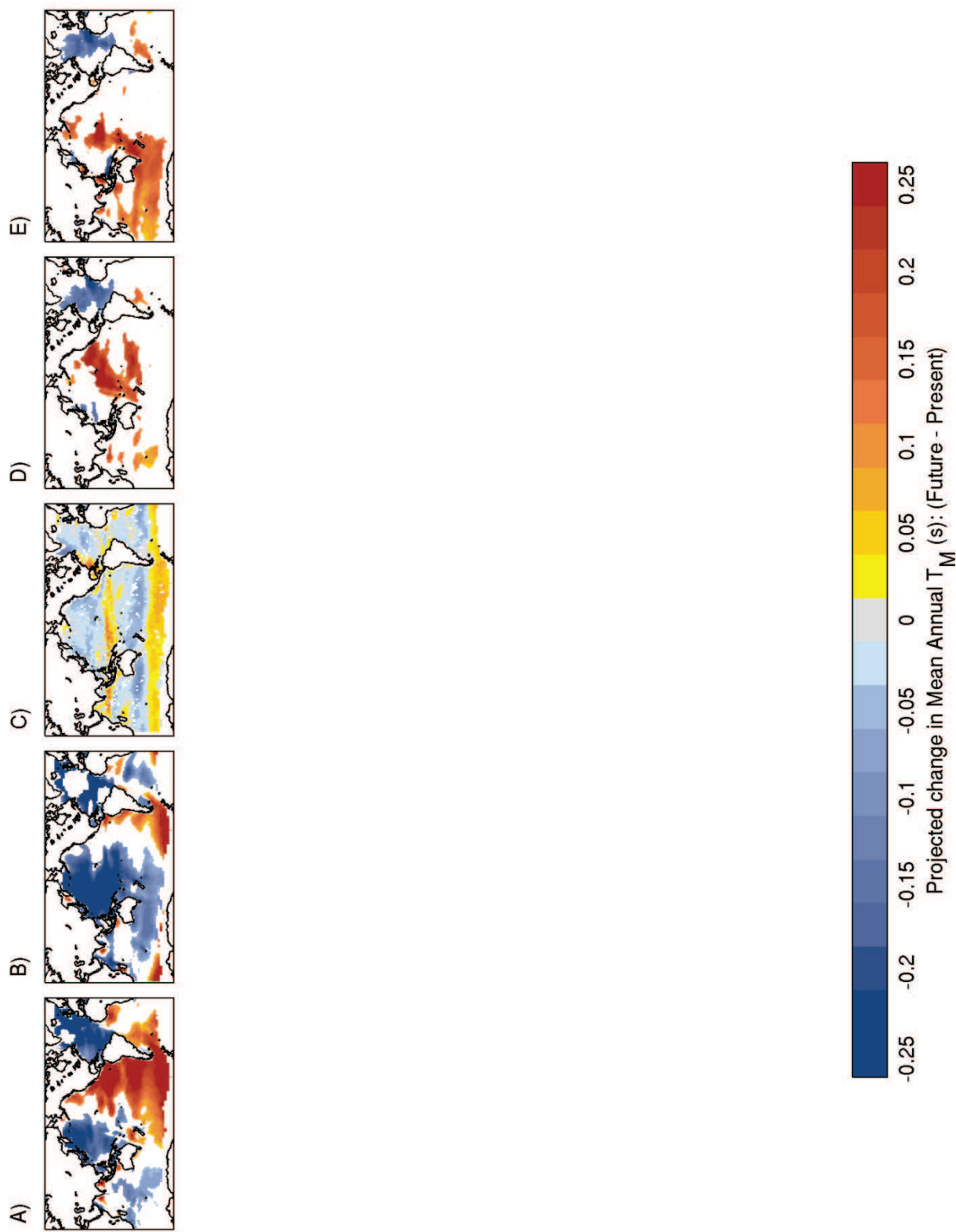


Figure SM9

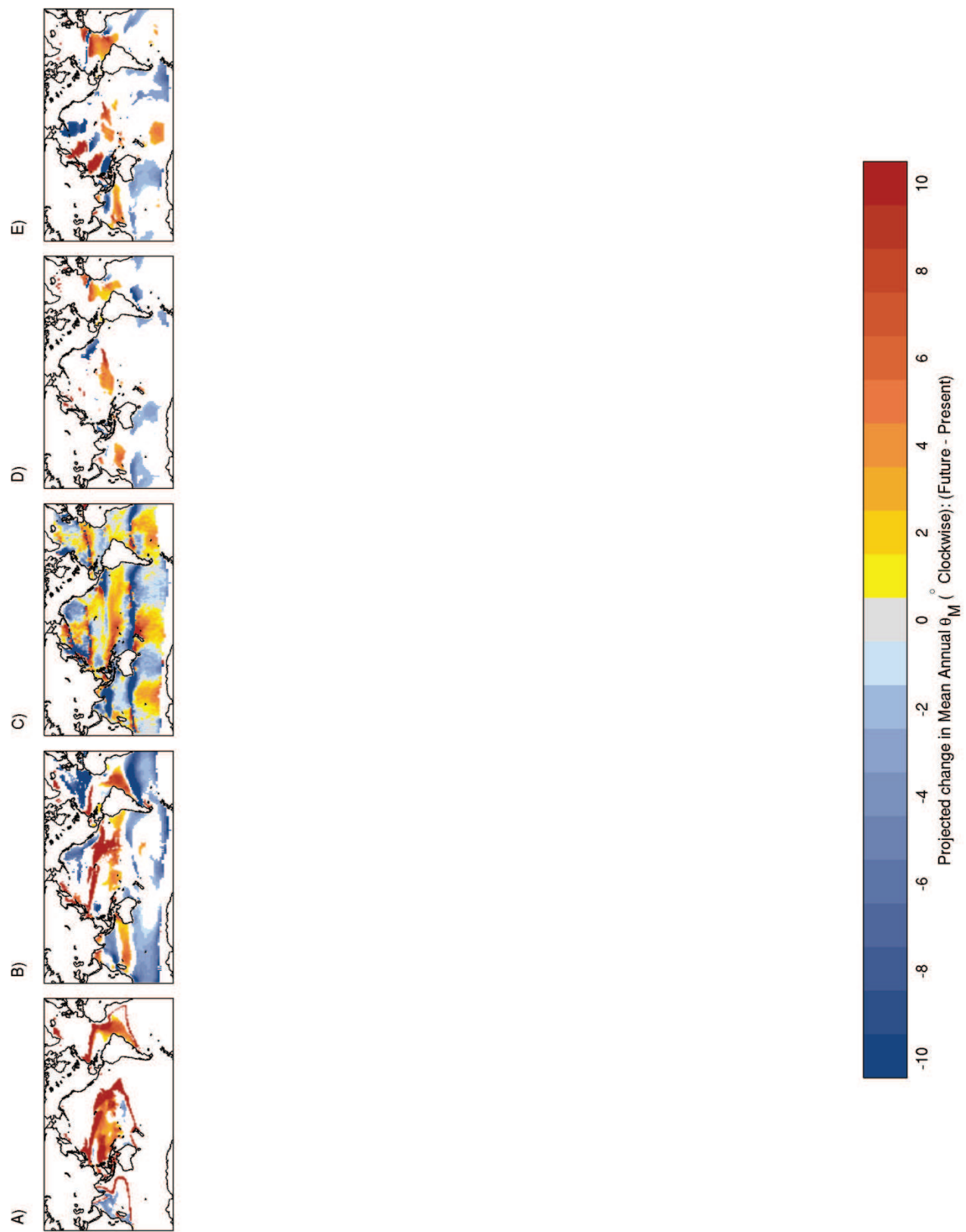


Figure SM10

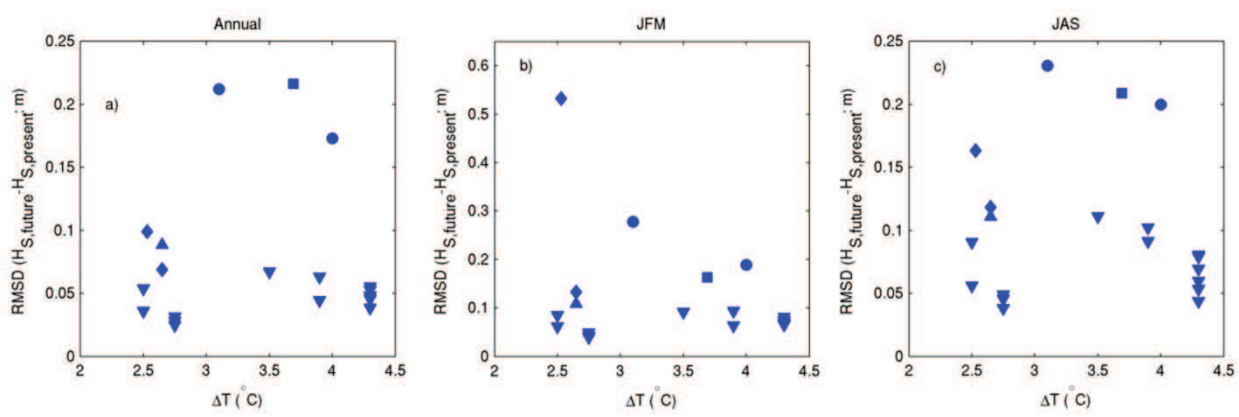


Figure SM11

Becky Summers

Wave heights will increase in seas off Indonesia, Antarctica and Australia's east coast, and will decrease in some other regions, an international collaboration reports today. The study looked into the effects of climate change on waves in the coming century, which may have implications for the fishing industry as well as for coastal mitigation efforts.

Waves mediate the continuous exchange of heat, energy, water vapour and gases between the atmosphere and ocean. They continually change in height, frequency and direction, influenced by wind and other factors that are in turn affected by climate patterns.

In the new study, published today in *Nature Climate Change*¹, the researchers projected wave attributes for the next century using five independent wave-climate models. They adjusted parameters in the models for predicted changes in the global climate, such sea surface temperatures, following the Special Report on Emissions Scenarios of the Intergovernmental Panel on Climate Change.

The study concluded that wave heights will increase in areas such as parts of Indonesia, the Southern Ocean and Australia's east coast, following shifts in the southern annular mode — a ring of climate variability that encircles the South Pole — and a strengthening of westerly winds in the Southern Ocean.

The researchers also predict a decrease in wave height for more than one-quarter of the world's oceans, particularly in the Northern Hemisphere. The cause may be a northward shift of Pacific high pressure.

Calmer seas in the North Atlantic will make major shipping routes safer, says study co-author Nobuhito Mori, a wave dynamics researcher at Kyoto University in Japan, and will also give deep-sea fishermen a reason to cheer — the industry requires wave heights to be smaller than 2–5 metres, depending on the size of the boat.

Coastal impacts

Coastal areas will be affected, as waves shape beach profiles and morphology. "When waves get smaller in the North Pacific, it means there will be less wave energy hitting the beach, and hence less beach erosion," says study co-author Yalin Fan, an atmospheric scientist at Princeton University, New Jersey. Smaller waves will also mean less energy for wave-power industries.

The study raises important questions about how to quantify the effects of climate change at the coast, says Judith Wolf, a coastal oceanographer at the National Oceanography Centre in Liverpool, UK. "The projected effects of climate change on wave heights are at least as important for coastal impacts in many areas as increasing sea levels," she says.



Australia's Gold Coast will see significant increases in wave heights in the next century.

BRUCE MILLER

1. Hemer, M. A., Fan, Y., Mori, N., Semedo, A. & Wang, X. L. *Nature* advance online publication, <http://dx.doi.org/10.1038/nclimate1791> (2013).

Show context

Comments

d w gregg said: Aside from the climate ideology drum beating, the studies I recall from the Little Ice Age compared to the Medieval Warming found that the Little Ice Age had a significantly greater number of more powerful storms in both recorded history and the geological record.

This makes sense if the climate system is viewed as a heat engine and the computer models are right, since if most of the warming takes place toward the poles and little in the tropics, there is less "tension in the climate spring." Less tension in the heat exchange engine should mean a

trend to fewer and weaker storms.

Yeah, I know this is not the political dogma.

2013-01-15 01:00 AM

Charles Raymond said: Curious--do you have a source/link for your information regarding the LIA and MW comparison?

2013-01-27 07:02 AM

Andreea Hill said: I think its suffice to simply say the human cost per ton of carbon emitted if prohibitively high. Lets look at it this way, if we lose our polar ice caps, the Earth will start warming uncontrollably because ice reflects sunlight while water absorbs the heat from the sun's rays. Its called "positive feedback". So we get even warmer because of the warming.

Next we start melting the tundra in Siberia which leads to methane releases, another positive feedback. So the warming makes even more warming.

Next the ice sheets (2500 metres thick) on Greenland start melting and when they are fully melted sea level goes up by 7 meters displacing 600 million people who live in low lying areas around the world.

Meanwhile we have been getting 100 year storms (like Sandy which caused \$60 B in damage) every year. And we have had crop failures in the US and Australia causing Global starvation and soaring food prices. I have done all this without a computer model and I don't think we need one. Some things are so obvious that even a politician should be able to figure it out without a calculator.

You need to be registered with *Nature* and agree to our Community Guidelines to leave a comment. Please log in or register as a new user. You will be re-directed back to this page.

See other News & Comment articles from *Nature*

Nature ISSN 0028-0836 EISSN 1476-4687

© 2013 Nature Publishing Group, a division of Macmillan Publishers Limited. All Rights Reserved.
partner of AGORA, HINARI, OARE, INASP, CrossRef and COUNTER